Computers and Geotechnics 160 (2023) 105510

Contents lists available at ScienceDirect

Computers and Geotechnics

journal homepage: www.elsevier.com/locate/compgeo

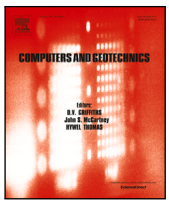

Research paper

Towards a more accurate characterization of granular media 2.0: Involving AI in the process

Stefano Buitrón Cevallos [c], Alex X. Jerves [a,b,c,*], Utkarsh Mital [d], David A. Medina [c], V. Santiago Quinteros [a,c], Maurizio Mulas [e], Øyvind Torgersrud [a]

[a] Advanced Numerical Modelling, Norwegian Geotechnical Institute, Oslo, Norway
[b] Facultad de Ciencias, Ingeniería y Construcción, UTE, Quito, Pichincha, Ecuador
[c] Fundación INSPIRE, INSπRE, Quito, Pichincha, Ecuador
[d] Earth and Environmental Sciences Area, Lawrence Berkeley National Laboratory, Berkeley, CA 94720, USA
[e] Facultad de Ingeniería en Ciencias de la Tierra, Escuela Superior Politécnica del Litoral, ESPOL, Guayaquil, Guayas, Ecuador

ARTICLE INFO

Keywords:
Granular materials
x-ray-CT scanning
Image processing
Level set
Convolutional neural network
Virtual laboratory testing

ABSTRACT

We introduce a Convolutional Neural Network (CNN) to reduce grains' manual inspection time after image processing on raw 3D x-ray computed tomography (3DXRCT) images from a sample of granular material to obtain level-set function-based digital twins of individual grains. The CNN automatically distinguishes properly segmented digital grains with up to 90% of accuracy. This algorithm is trained using, ground-truth, level set-based digital grain representations from a natural soil sampled at Jaramijó (Ecuador). The implemented convolutional neural network provides groundbreaking processing power, reducing the, otherwise, manual inspection time expended for a small sample, e.g., 200 000 grains, from approximately a couple of weeks to only a few hours. Furthermore, transfer learning and training from scratch are compared for artificially graded granular materials such as Øysand (Norway) and Hostun sand (France). The CNN's learning process is interpreted by means of grain morphological parameters, i.e., sphericity, roundness, grain diameter, and volume-surface ratio. Hence, being able to automatically segment a greater amount of grains from 3DXRCT images of natural and artificial soils in a short period of time, enables us, for first time, to perform actual 3DLS-DEM-based virtual laboratory testing (a plug-and-play one-stop shop). Providing unprecedented and unique data for engineering applications.

1. Introduction

Image processing is a powerful tool for the study of granular materials related phenomena such as failure, shear banding, critical state, and dilation (Jerves et al., 2019). For example, to obtain a digital representation of a soil sample, a 3D X-Ray Computed Tomography (3DXRCT) is needed. Then, the grains are extracted from the tomography with image processing algorithms. Studies with the obtained grains contribute in engineering and space exploration. In engineering, the digital grains can be used for accurate soil characterization (e.g., by computing the morphological parameters defined in Cho et al., 2006) and mechanics (Cheng and Wang, 2018; Sivakugan et al., 2015; Daub et al., 2010), which, in turn, are important for the construction industry. In space exploration, study of granular materials may help address the issues related to the abrasive effects of charged particles on equipment, exploration vehicles and fabrics of space suits (Stubbs et al., 2007). Some of the aforementioned image processing algorithms have first been developed for medical applications like Magnetic Resonance Imaging (MRI). For example, on accurate image segmentation (Dill et al., 2015; Liu et al., 2021; Kim et al., 2013) and morphological measurements of organs and tissues such as the brain's hippocampus to help to an early diagnosis of dementia and cognitive impairment (Uhl et al., 2018).

In the context of granular mechanics, image processing techniques have been used, for example, to characterize inter-particle contacts for granular materials with watershed algorithms on 3D binary images (Viggiani et al., 2013; Andò et al., 2013). Similarly, level set (LS) functions have proven effective not only to capture arbitrary grain shapes from tomographic images, but also to be used for discrete element method (DEM) simulations (Vlahinić et al., 2014, 2017). In addition, novel μ-XRCT provides high resolution images that combined with threshold-based image segmentation, contribute to increase the segmentation accuracy of grains in contact (Wiebicke et al., 2017).

* Corresponding author at: Advanced Numerical Modelling, Norwegian Geotechnical Institute, Oslo, Norway.
E-mail address: alex.xavier.jerves@ngi.no (A.X. Jerves).

https://doi.org/10.1016/j.compgeo.2023.105510
Received 10 January 2023; Received in revised form 24 April 2023; Accepted 30 April 2023
Available online 24 May 2023

Moreover, a novel toolbox that is often used for analysis of granular materials' images is the Software for the Practical Analysis of Materials (SPAM), a Python package developed in Grenoble (Stamati et al., 2020).

In the realm of artificial intelligence and machine learning applied to the study of soil and granular materials, so far, the focus has been put on tasks such as establishing an alternate segmentation process to the otherwise well-established procedures (i.e., thresholding or watershed-based segmentation). For example, the implementation of a Convolutional Neural Network (CNN) based U-net model for 3DXRCT image segmentation of 7 different soil samples. The 3DXRCT grayscale and binarized images were considered as their ground-truth data, reporting that the segmentation error varied from 5% to 130%, depending on the granular material (Lavrukhin et al., 2021). Furthermore, a similar work uses a machine learning technique called Trainable Weka Segmentation to segment 3DXRCT images, having obtained 77% of grains from a small soil sample tomography of Mojave Martian Simulant (Lai and Chen, 2019). Another application has been implemented for urban and agricultural use of soils, with the classification of different land covers with a CNN model. However, instead of 3DXRCT images, the classification is performed from spectral measurements acquired by visible near-infrared spectroscopy technology. The CNN classification accuracy is above 87% (Li et al., 2021).

Finally, it is worth mentioning that there are several devices for size and morphological characterization of fine-particulate materials, which are based on laser diffraction and the angle of light scattered by a stream of particles passing through a laser beam, the so-called particle size analyzers (CompareNetworks, 2009).

In this work, an image segmentation technique to obtain level set-based grains from raw 3DXRCT images of a soil sample is followed, facing common problems such as oversegmentation and undersegmentation in the process. Researchers have worked on this problem and proposed different solutions, however, image processing algorithms can still be improved in order to successfully segment more grains from the tomography. The aforementioned research projects were carried out in an effort to answer a fundamental question: *Is it possible to create a scheme/framework for image processing capable of processing soil sample's grains obtained from 3DXRCT regardless of their morphology, i.e., size and shape?*.

Incorrectly segmented level set-based grains from image processing need to be discarded, requiring manual visual inspection. This inspection is a long, repetitive, time consuming, tedious and error prone task because small "academic" soil samples normally contain from 2,000 to 100 000 grains that need to be inspected one by one. Thus, the fundamental goal of this project is to *develop an algorithm that automatically detects properly segmented digital grains from a real soil sample or, at least, that reduces manual inspection time*. The main interest in keeping only the correctly segmented grains is to use them for 3D level set discrete element method (3DLS-DEM)-based virtual laboratory simulations (Jerves et al., 2016; Medina and Jerves, 2019; Bustamante et al., 2020).

Fig. 1 sketches the improvements incorporated into the design of the image processing algorithm discussed by Vlahinić et al. (2014), and used to obtain digital grains from raw 3DXRCT images of natural and artificial soil samples. The main added improvement is a CNN classification model that substitutes the manual inspection of segmented grain images. A soil sample from a given location of interest is extracted, Fig. 1(a). Then, the sample of Fig. 1(b) is 3DXRCT-scanned in a laboratory facility, Fig. 1(c). The original image processing algorithm is used (Fig. 1(d)), obtaining "faithful" and ill-segmented digital level set-based grain representations, Fig. 1(e).

A total of four improvements are included in the original algorithm, i.e., a contrast limited adaptive histogram equalizer (CLAHE) (Zuiderveld, 1994), tiny local minima filtering (Soille, 2000), a filling algorithm tool for holes in a binarized image, and the calculation of the centroid from each individual grain, Fig. 1(f).

Regarding the aforementioned CNN classification model, it is trained by using a ground-truth dataset of manually inspected "faithful" and ill-segmented level set-based grain representations. The person in charge of the manual inspection procedure needs to bear enough knowledge and experience to accurately identify most of the properly segmented digital grains. This may be a long learning process, taking at least several weeks of continuous training. Once the training has finished, the average time that takes to visually inspect one grain is approximately 5 s. Nevertheless, the introduced convolutional neural network rises as a powerful, user friendly, tool, that radically reduces the training process to a couple of hours. Once the CNN is trained, the average time that takes to automatically classify one grain is around 5×10^{-3} s, being at least 1000 times faster, with an accuracy up to 90%.

Moreover, in order to ensure the reliability of the model we use four different soil samples, with varied morphological characteristics (large, small, rounded, angular), to train and test the CNN. The samples include a natural soil from Ecuador (Jaramijó sand), and three artificially modified soils from United States (Martian Regolith Simulant), France (Hostun sand) and Norway (Øysand). Furthermore, an attempt to interpret the learning process of the CNN is performed, taking an educated guess based on the morphological characterization of the automatically classified grains by the CNN. Finally, properly processed grains can be used for analysis and 3DLS-DEM-based virtual laboratory simulations, Fig. 1(h).

The present work is divided in four sections. As depicted by Fig. 1, the first section details the steps of the original image processing algorithm, followed by the applied improvements (see Fig. 1(f)). In the second section, the proposed CNN architecture is detailed (see Fig. 1(g)), which was evaluated by means of accuracy, precision, recall and F1-scores with digital grains of Jaramijó's sample. In the third section, morphological parameters of the predicted digital grains from Jaramijó are calculated to interpret the CNN's learning process. In the last section, the CNN was tested with other granular material than the one used to train it, such as "faithful" digital Martian Regolith Simulant grains, as a first attempt to estimate the scope of the CNN. Next, training from scratch and transfer learning were evaluated as methods to train the CNN with other granular materials, e.g., digital grains from artificially graded soils like Øysand and Hostun sand Wiebicke (2020), comparing the metrics to determine which method has better classification results.

This work and its results aim to be part of a process that seeks to automate and industrialize 3DLS-DEM-based virtual laboratories (a one-stop shop). This, through material morphological characterization and physics-based simulations, can unravel the micro- and nano-mechanics that furnishes the microscopic behavior of granular materials, providing unprecedented and unique physical and morphological data. The process starts from a raw 3DXRCT image of any type of soil sample, and ends with the "faithful" level set-based grains automatically selected by the CNN to, then, be used in 3DLS-DEM-based simulations.

Finally, nowadays, one significant shortcoming in the study of granular materials is the lack of available, consistent, and well-documented databases. Scarce databases for natural or artificial soils exist around the world. However, these databases often lack information about the samples' geographic location, classification of the material, phenomenological parameters such as friction angle and cohesion, morphological parameters, e.g., roundness and sphericity, or state parameters such as porosity and water content. These databases are very scarce as well as scattered worldwide. Hence, this work attempts to help triggering the automation and industrialization of 3DLS-DEM-based virtual laboratories, enabling the creation of novel databases that not only host the aforementioned information, but also drastically diminish the need for sampling. Thus, once a digital twin sample is casted from a physical sample, the twin can be reconfigured at will by changing its so-called state parameters and performing as many virtual tests as desired.

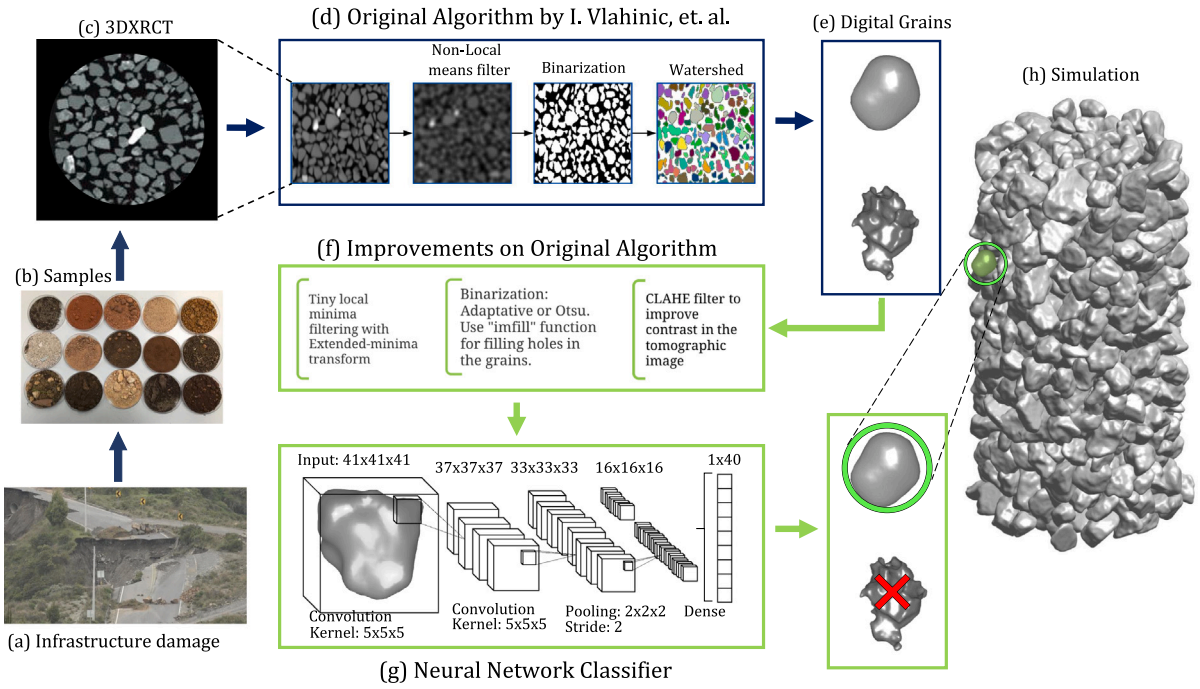

Fig. 1. Digital grains' processing and classification procedure: first, a real soil sample is extracted from (a) a location of interest. (b) A sample is then scanned with the aid of a (c) 3DXRCT to obtain raw images of the grains. (d) These are then processed through the image processing algorithm proposed by Vlahinić et al. (2014), nevertheless, it produces as outcome (e) some properly and improperly segmented digital grains. (f) Improvements are applied on the original algorithm, nevertheless, some digital grains still need to be manually inspected. For that reason, (g) a Convolutional Neural Network (CNN) is proposed to automate this time consuming operation. In this case, the CNN is trained with an input dataset of properly and improperly segmented level set-based grains, obtained after a visual inspection and manual labeling of the two mentioned categories is carried out. Further, the CNN's hyperparameters are fine-tuned to achieve a highly efficient classifier that successfully eliminates improperly processed grains. Finally, (h) the resultant properly processed grains of the digitized sample can be incorporated in 3DLS-DEM-based virtual laboratory simulations for the study of morphological and physical phenomena such as failure, shear banding, critical state and dilation.

2. Image processing algorithm

A briefly description of each step in the algorithm by Vlahinić et al. (2014) is provided, starting from the image processing of raw 3DXRCT images of a soil sample to the generation of a 3D level set (LS) representation of each grain in the tomography. Then, four proposed improvements to the algorithm are detailed, which includes two additional filters, a filling algorithm for binarized images, and the centroid calculation of each grain in the 3DXRCT image, detailing important calibration parameters in order to reduce the number of incorrectly processed grains.

2.1. Original algorithm

Vlahinic's image processing algorithm describes five consecutive steps to obtain the 3D level set (LS) representations of individual grains from a raw 3DXRCT image. First, 2D radiographs of a soil sample are reconstructed to a 3D volume using the filtered back projection technique slice by slice, obtaining the raw 3DXRCT grayscale image. Second, the raw 3DXRCT images are enhanced by a non-local means denoising filter, which helps to preserve details on phase/grain boundaries. Third, phases (i.e. voids, grains, or water) are identified in the denoised 3DXRCT grayscale images by a thresholding technique that analyzes the histogram of pixel intensities, giving a binarized image as result. Fourth, each individual grain in the binarized image is segmented and labeled by means of a watershed algorithm, which computes the distance map in the binary image and expands the "islands" (local maxima or minima) until each grain boundary is reached (Digabel and Lantuejoul, 1978; Vincent and Soille, 1991). Then, a division line in grains that are in contact is created depending on the implemented watershed algorithm. Finally, an initial guess for each individual grain is generated from the watershed labeled image. Then, this is used as input for a distance regularized level set evolution (DRLSE) scheme (Li et al., 2005, 2010). Hence, level set-based mathematical representations are obtained for each grain Kawamoto et al. (2016).

Vlahinic tested the algorithm on 3DXRCT images of artificially modified soil samples such as Hostun sand or Caicos ooids, which are made of uniformly graded grains. However, the initial focus of this work was to test the algorithm in a well graded natural soil with varied grain diameters and shapes, such as the grains from Jaramijó's sand.

This natural soil sample is extracted from a beach located in the town of Jaramijó, Ecuador. In Fig. 2(a), a single slice from the raw 3DXRCT image of Jaramijó' s sand is displayed, with angular, rounded, small and large grains. For instance, the grain diameters range from 0.002 mm to 1 mm (see Fig. 7), with a maximum to minimum ratio of 500. For a more detailed description of the sample's gradation, see Section 2.2 and Fig. 7.

Thus, the image processing algorithm (described above) was used as well as fine tuned to process a 500x500x1000 voxel 3DXRCT image taken from a sample of Jaramijó' s sand. Then, the resultant level set-based grains where manually checked (as detailed in Section 2.2), finding that only 43% were properly processed, i.e., these grains are faithful representations of their physical counterpart. Hence, these results were the main motivation to improve the image processing algorithm, with the objective to achieve a higher segmentation accuracy on raw 3DXRCT images of natural soil samples as well as artificially modified soil samples.

2.2. Algorithm improvements

First, as an introduction for this section, it is worth mentioning that all the steps shown by Fig. 4 are based on the Matlab Image Processing Toolbox. Second, the main four additions made to the original algorithm by Vlahinić et al. (2014) for this work are: the Contrast Limited Adaptive Histogram Equalization filter (step 1 in Fig. 4), hole filling algorithm in binarized images (step 4 in Fig. 4), tiny local minima

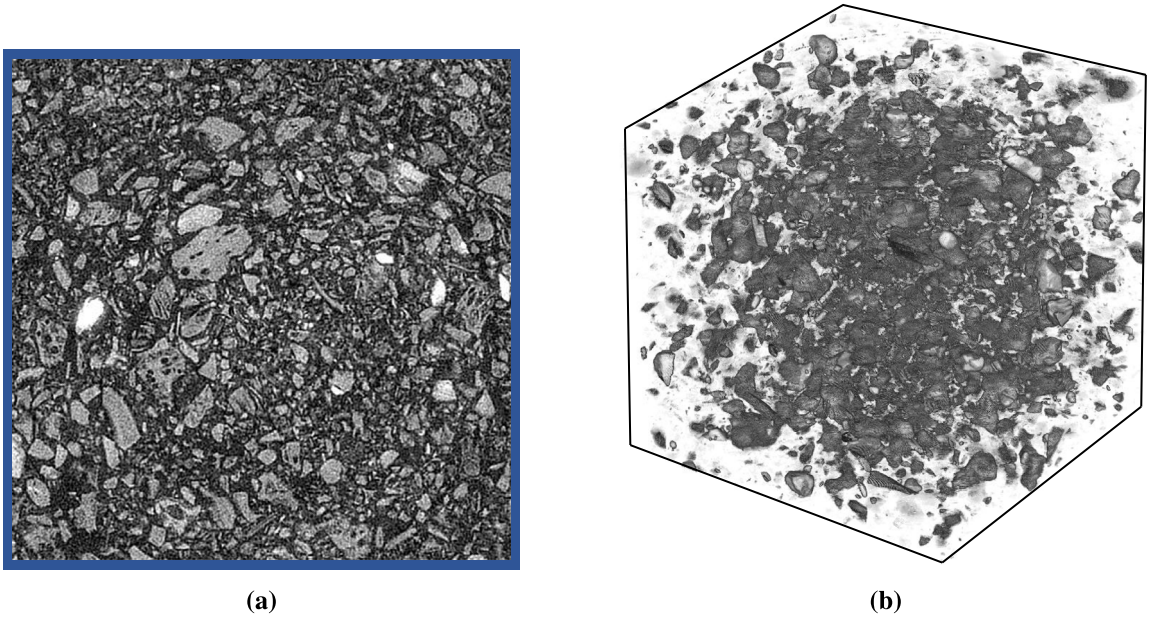

Fig. 2. (a) A single slice from a raw 3DXRCT image of the soil sample extracted from Jaramijó, displaying round, angular, small and large grains. (b) 3D representation of 500 slices from the raw 3DXRCT image of Jaramijó's soil.

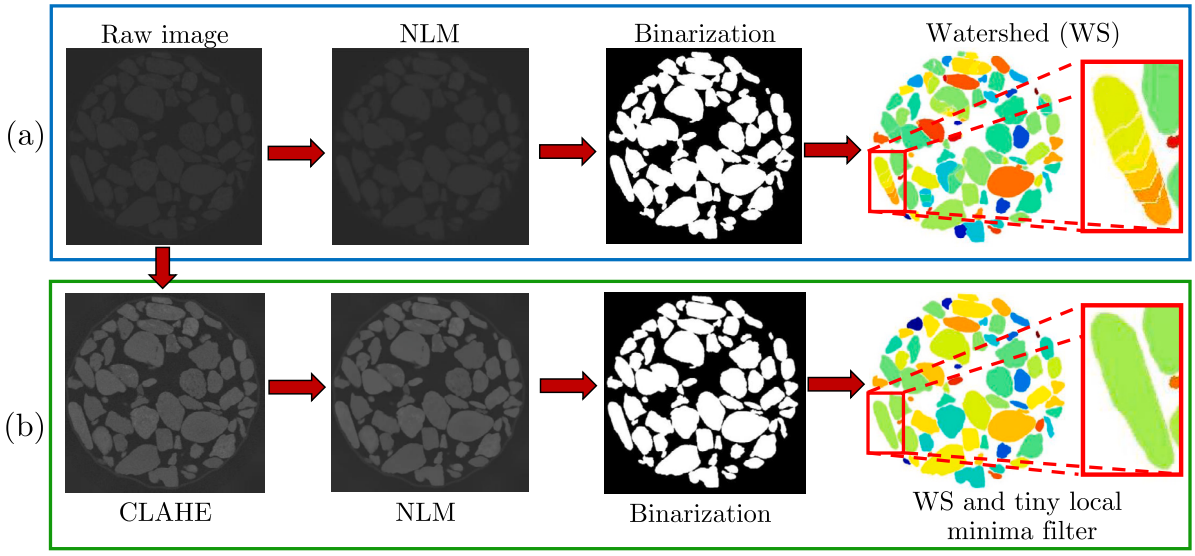

Fig. 3. (a) Image processing with the original algorithm. (b) Image processing with the improved algorithm.

filtering (step 5 in Fig. 4), and grains centroid calculation (step 7 in Fig. 4).

The Contrast Limited Adaptive Histogram Equalization (CLAHE) filter (Zuiderveld, 1994) makes it easier to identify grain borders, when the images are binarized, by improving the contrast between grains and voids in the 3DXRCT scans. The objective of this filter is to redistribute the brightness values across the image to reduce the noise in it. The CLAHE filter needs a contrast parameter as input. With this filter, the amount of grains that are mistakenly joined together during binarization is reduced, as shown in Fig. 3.

A common error of the watershed algorithm is oversegmentation (see Fig. 3(a)), caused when more than one local minima in the same grains are calculated in the distance map. To reduce the oversegmentation error, tiny local minima was filtered by applying extended-minima transform (Soille, 2000). As consequence, a single local minima on the grain is ensured, reducing the probability of the watershed algorithm to draw segmentation lines in the same grain. One drawback of tiny local minima filtering is that the minima of one grain may match a value from other grain, merging them together and labeling it as a single one (undersegmentation). The filter was tested with denoised 3DXRCT scans of Øysand (Norwegian sand), determining that the amount of fixed oversegmented grains was higher in contrast with undersegmented grains caused by the filter, as seen in Fig. 2(b).

The above listed additions were tested and validated with three sands, namely the Ecuadorian (Jaramijó sand), Norwegian (Øysand) and French (Hostun sand), following the algorithm in Fig. 4, where the parameters have to be calibrated for each soil sample (see Appendix).

1. A raw 3DXRCT image can be improved applying the CLAHE filter with the Matlbab function "adapthisteq". The "adapthisteq" function controls the contrast with the "ClipLimit" parameter,

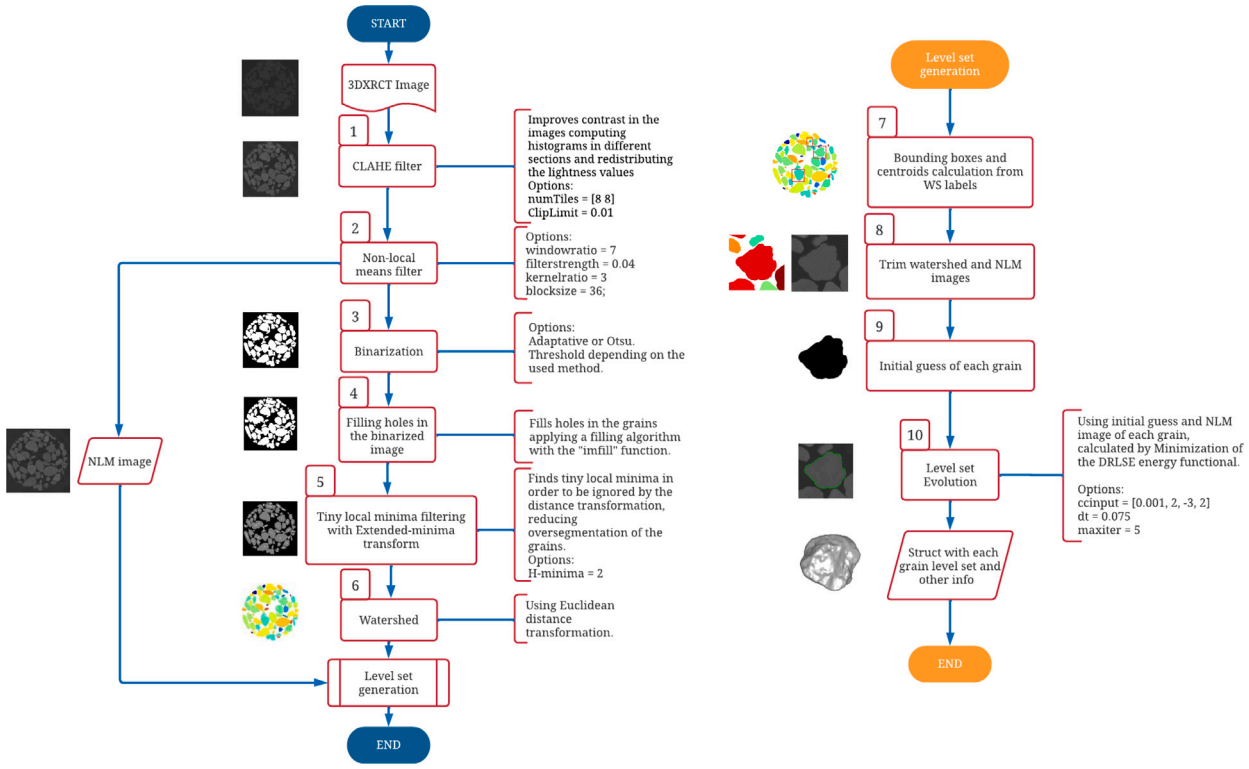

Fig. 4. Flowchart of the algorithm to generate level set-based digital twins of individual grains from raw 3DXRCT images. The parameters specified within each step of the Flowchart were calibrated for 3DXRCT images on a sample from Øysand (Norway). This calibration is also used as a basis for parameters customization on 3DXRCT images from Jaramijó (Ecuador), and Hostun sand (France) samples.

which is calibrated through trial and error, since a bigger value may make the image too bright or a small one will not give enough brightness. As per in Fig. 4, a clip limit value of 0.01 worked fine with the tested images.

2. A non-local means filter accepts as input the CLAHE filtered image. The parameters of the filter determines the volume of voxels (or window) to be analyzed with its neighbors. The parameters specified in Fig. 4 were selected considering processing time and memory usage constraints (i.e., a higher filter strength helps to reduce noise, but the filter takes more time to process).
3. A thresholding binarization method is applied to the non-local means denoised image, changing grains pixels to 1 and void pixels to 0. In this study, the threshold was determined using either global methods such as Otsu (1979), or local schemes such as Adaptive (Bradley and Roth, 2007) with the "imbinarize" Matlab function.
4. Voids inside the grains can be fixed with the Matlab function "imfill" (Soille, 2004), which applies a filling algorithm (see Fig. 4) based on morphological reconstruction, analyzing the location and connectivity of void pixels to obtain as output a binary image.
5. The process of grain segmentation starts with the tiny local minima filtering with extended minima transform, implemented with the Matlab function "imextendedmin", which finds tiny local minima in the distance map and eliminates it in order to be ignored as islands, reducing oversegmentation. The parameter that determines the filtering is H-minima, calibrated by trial and error depending on the soil sample. A similar process can be performed by using the adaptive watershed described in Sun and Luo (2009).
6. The Fernand Meyer watershed algorithm (Meyer, 1994), implemented with the Matlab function "watershed", is applied in the distance map filtered with the extended-minima transform, identifying each individual grain as an island and labeling them with a number, having a total number of labels equal to the total number of grains.
7. Both non-local means filtered and watershed segmented images are used as input for the level set generation, but first, it is necessary to separate each grain in these images. For this, the global coordinates of each bounding box containing a single grain are determined. In parallel, the global coordinates of each individual grain's centroid are calculated from the watershed labels as follows: first, the grain is located with its given label in the watershed segmented image. Then, a zero value is assigned to all the voxels with other labels, and a value of one to the voxels with the label of that grain. Finally, the means for all x, y and z positions of the grain voxels are computed, giving as result the global coordinates of the grain's centroid.
8. With the coordinates of the bounding boxes, watershed segmented and non-local means filtered images are trimmed to separate each grain. In this step, the center of mass of each grain is saved for later re-processing when needed.
9. The level set evolution process starts with the initial guess of a grain, binarizing the trimmed watershed segmented image with an initial binary function.
10. The algorithm ends with the level set evolution, using the parameters specified in Fig. 4 and, as input, the initial guess done with the watershed label of a grain, paired with its corresponding non-local means filtered image. The evolution is done until a DRLSE energy functional is locally minimized. As output, data, such as the level set matrix, centroid, and bounding box's coordinates, is obtained for each segmented grain from the 3DXRCT image.

The described algorithm was tested with the same 3DXRCT image of the natural soil sample from Jaramijó' s sand previously processed with the original algorithm (described in Section 2.1). In order to compare the results, the parameters for filters, such as the non-local

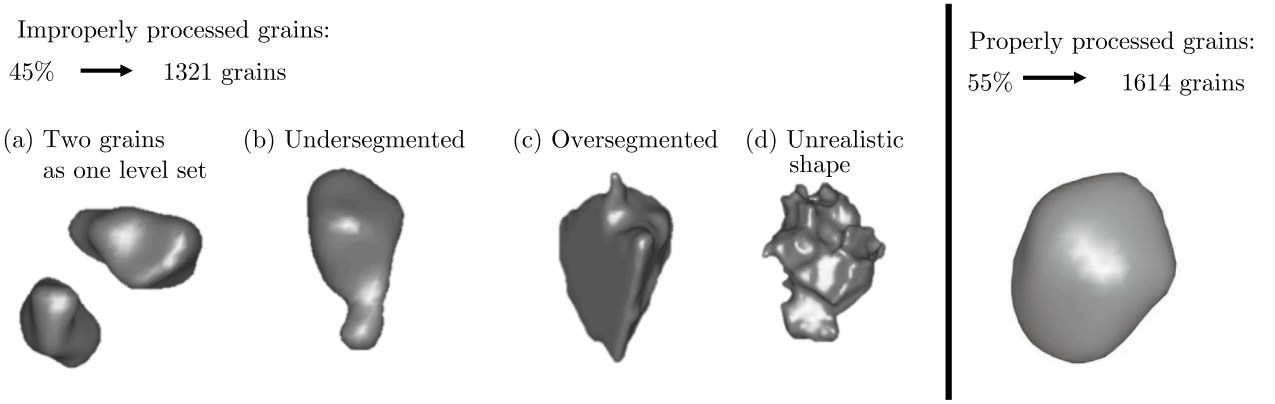

Fig. 5. Types of defects in the image segmentation process described by Fig. 4 to go from raw 3DXRCT images of a real sample of Jaramijó's soil to individual level set-based digital grain avatars: (a) Individual parts are given the same label during the semantic segmentation process, and finally coming up as one level set function, (b) typical undersegmentation case caused by different grains in contact being recognized as a single one, (c) typical oversegmentation case caused by a single grain split into several parts, and (d) unrealistic shapes caused by the detection of voids, noise, or grain clustering. From 2935 digital grain avatars, 45% of them display some kind of defect, and 55% corresponds to the properly processed digital avatars.

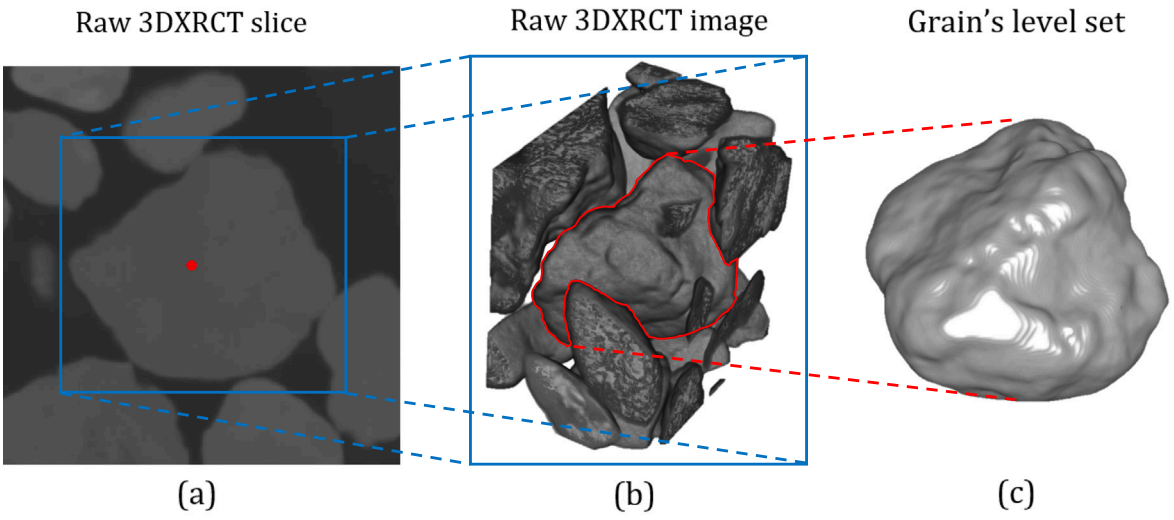

Fig. 6. Visual examination procedure followed for each grain's level set representation: (a) individual localization of the grain's level set in the raw 3DXRCT image by means of its centroid coordinates, (b) 3D visualization of the corresponding raw 3DXRCT image, and (c) visual comparison of the grain's level set representation to the raw 3DXRCT image.

means filter, were the same in both algorithms. The original image processing algorithm yielded 43% of correctly processed level set-based grains, however, the improved image processing algorithm gives 55% of correctly processed digital grains, representing an improvement of 12%.

To determine the percentage of properly segmented digital grains, and discard the improperly segmented ones, all of the level set-based grains were manually classified, one by one, as described below. In Fig. 5 some defects corresponding to the incorrectly processed grains are displayed.

2.3. *The manual inspection protocol (ground-truth)*

The manual inspection procedure is as follows: first, a visual examination of each grain's level set representation is carried out. During the examination, the grains are individually localized in the raw 3DXRCT image by means of their centroids coordinates, described in step 7 of Fig. 4. Then, the level set representation is compared to the raw 3DXRCT image, as shown in Fig. 6, assuring that the level set does not show errors such as oversegmentation or undersegmentation.

Second, once manual classification has finished, all of which are considered as "faithful" level set representations are computed their morphological parameters (Cho et al., 2006; Jerves et al., 2016; Medina and Jerves, 2019), i.e., grain's diameter, aspect ratio, sphericity, roundness, volume, and surface area, as defined by Eqs. (5)–(7). Then, the cumulative grain size distribution from the digital "faithful" grains is obtained and validated with respect to its counterpart from the physical laboratory (see Fig. 7). Previously, the real sample grain size distribution has been acquired by the physical laboratory using the following procedure: the grain size distribution ranging between -11ϕ and -4ϕ (ϕ = -log2d, where d is the grain diameter in mm) was determined by area image analysis. The sample was dry-sieved from -4ϕ to 4ϕ (1ϕ interval), and from 4ϕ to 11ϕ the grains size were determined by Laser Scattering Particle Size Distribution Analyzer (LA-300 Horiba) (Roverato et al., 2018).

Third, after validation with respect to the physical laboratory grain size distribution, a final validation is performed to discard the grains whose diameter is too close to the 3DXRCT resolution (smaller than 15 times the 3DXRCT scan resolution). This final step is carried out because the grains whose sizes are too close to the 3DXRCT resolution tend to yield wrong values of their other morphological parameters and induce numerical errors on 3DLS-DEM-based simulations. *Unlike other works* (Lavrukhin et al., 2021; Lai and Chen, 2019), *here the 3DXRCT grayscale and binarized images are not used as the ground-truth data.*

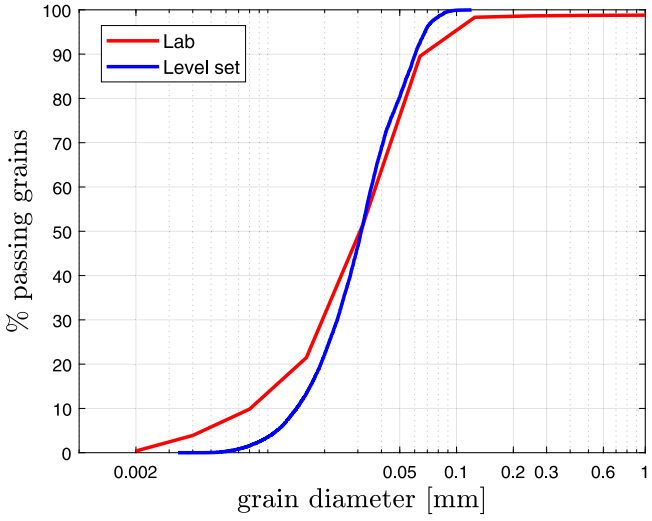

Fig. 7. Grain size distribution of 1000 Jaramijó grains. Digital grains (blue line), and physical laboratory results (red line).

Instead, the remaining "faithful" level set-based grain representations are considered as the ground-truth for training and testing the Convolutional Neural Network described in the following section.

Furthermore, from a more in depth analysis of Fig. 7, the level set-based Jaramijó grains yield a coefficient of uniformity $C_u = D_{60}/D_{10} = 2.49$ and a coefficient of curvature $C_c = D_{30}^2/(D_{10} \times D_{60}) = 1.08$. On the other hand, the real sample yields a $C_u = 4.82$ and $C_c = 1.17$, where D_{10}, D_{30}, and D_{60} are the grain diameters at 10, 30, and 60% passing, respectively. Both C_c and C_u are measures of soil gradation, they help to identify if a soil is well graded or poorly graded. Thus, for C_u, values between 4 to 6 determine a well graded soil, while lower values than 4 determine a poorly or uniformly graded soil. Moreover, values between 1 and 3 of C_c determine a well graded soil, while poorly otherwise. In the same way, it is worth noticing that even though C_u and C_c are both used as measures of soil gradation, C_c takes into account more information about the grain size distribution (it also includes D_{30}), giving a more accurate measurement.

Hence, from the last paragraph and Fig. 7, it can be inferred that C_u from the digital grains gives an error of 48.22% with respect to the real sample. However, the error for C_c is 7.45% only. This suggests that the grain size distribution from the small digital sample (made of 1000 grains) shows physical and statistical convergence with respect to the real sample (439.6g ≈ 1 pound). The aforementioned convergence can also be noticed from Fig. 7, where the digital and real samples have similar values of D_{60}.

Finally, it is worth mentioning that for sand-like materials, discarding the grains whose diameters are smaller than 15 times the 3DXRCT scan resolution does not affect the level set grain size distribution curve, since these resolutions are orders of magnitude smaller than the average grain's diameter.

Remark

The value of 15 times the 3DXRCT scan resolution was determined so the roundness-scale (grain diameter/10) (Cho et al., 2006) can be fully captured. Hence, if the grain's diameter is smaller than ten times the 3DXRCT scan resolution, all the morphological information provided by the roundness is lost. Additionally, a security factor of 1.5 is considered to ensure a proper calculation of roundness values.

3. A neural network based grains classifier

Commonly used for image and video classification and analysis (Rawat and Wang, 2017; Guo et al., 2017; Xu et al., 2016; Burney and Syed, 2016), Convolutional Neural Networks (CNN) are characterized by its computational efficiency by reducing the amount of hidden layers, and its learning process that is constrained through spatial correlation. A CNN consists of convolutional operations which extract feature maps (Khandelwal, 2020) from the input data. Feature maps analyze important objects of interest from the data, e.g., first layers extract general information like edges, color (in case of a RGB input image), curves, etc., while later layers extract specific and detailed features. To build a CNN architecture or model, a group of layers and a set of hyper-parameters have to be specified. During the training process, these hyper-parameters (e.g., training rate, layers, activation functions, dropouts, number of neurons in a layer, and many others) are tuned until the best score is obtained, depending on the selected evaluation metric (i.e., accuracy, precision, recall, F1-score, etc.). CNNs have been used before for 3DXRCT image segmentation of different soil samples, considering the grayscale and binarized image as ground-truth for training (Lavrukhin et al., 2021). It has also been used for 3D sand particles generation as in Shi et al. (2021), and for sand type classification in 2D grayscale images (Kim and Yun, 2021).

As previously mentioned in Section 2.2, manual inspection of digital grains is a long and tedious process, subjected to human error, but necessary to discard badly segmented grains. Nowadays, however, a solution to this issue can be found in machine learning. In specific, CNNs offer a powerful tool that can be trained with the objective of automatically distinguish "faithful" digital representations of individual physical grains from their ill-processed counterparts, simplifying and optimizing the pipeline. Thus, in this case, the CNN would require for its training a binary classification, labeling the former group with a value of 1 (considered as our ground-truth) and the latter group with a value of 0. In favor of simplicity, from now on, we call them as "good" (properly segmented) and "bad" (ill-segmented) grains.

3.1. Convolutional neural network

For this work, the convolutional neural network was implemented in Python 3, aided by Keras, and TensorFlow libraries, using the free cloud services hosted by Google Colab. The free version of Google Colab offers a GPU with a runtime up to 12 h (prioritizing an interactive use), and it comes with an Intel Xeon CPU @2.20 GHz, 13 GB of RAM, a Tesla K80 accelerator, and 12 GB GDDR5 VRAM. The CNN arquitecture, described in Fig. 8, has the following structure:

- *1. Pre-processing:* to implement the neural network, input data must be pre-processed, in this case, 3D matrices (that correspond to the level set representation of each grain) are used. The network requires the level set function bounding boxes to be, first, normalized to the same size, i.e., 41 × 41 × 41, and then, their values mapped into an interval between zero and one by applying min–max normalization (Aksu et al., 2019).
- *2. Convolution block:* the CNN's architecture has a set of sequential layers grouped in two convolutional blocks (2a and 2b, respectively, in Fig. 8) that extract information from the input data. (i) The block 2a requires the specification of the input data size, i.e., one channel for the level set data, and one channel for each of the three RGB color bands. (ii) Two 3D convolutional layers are used to begin with the data analysis, extracting information. (iii) The weights of the network are normalized with a tanh activation function. (iv) A batch normalization layer is implemented to avoid overfitting (i.e., the CNN adapts well to the training data, however, predictions are poor with unknown data). (v) The most relevant features are extracted with a 3D max pooling layer, which reduces the size of the input level set matrix for the next

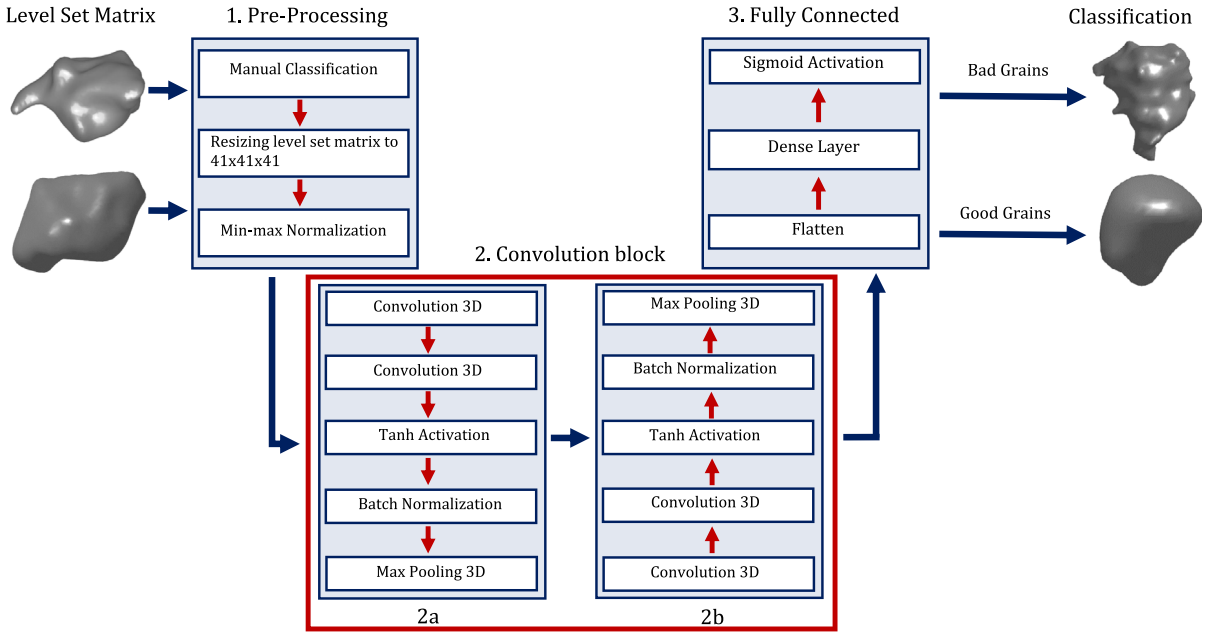

Fig. 8. Pre-processing of the grains' level sets and architecture of the implemented CNN, resulting on the binary classification of "good" or "bad" grains.

convolutional block. (vi) The block 2b has the same layers as 2a, and it is used to extract more specific features or details from the data.

- *3. Fully connected:* convolutional layers only extract information, but in the fully connected block it is where the predictions are made. The flatten layer takes the 3D output from the 2b convolution block and resizes it into a N-dimension vector. Then, a dense layer, where the hidden neurons are located, takes the weights from the N-dimensional vector to make a prediction. Finally, for a binary classification task (e.g., determining if a digital grain is "good" or "bad") a sigmoid activation function is required, having as output a probability between zero ("bad" grain) and one ("good" grain).

All of the manually classified digital grains were used as input data, consisting of 2500 Jaramijó digital grains in total, with imbalanced groups of 1000 "good" and 1500 "bad" grains. Then, 70% of the digital grains from each "good" and "bad" groups were randomly picked and used as the training set, while the remaining 30% was left for testing, in order to evaluate metrics, like accuracy, after each epoch. Metrics, such as precision and recall, are used with imbalanced data to evaluate the CNN, as suggested by Juba and Le (2019). The definitions of the metrics used for this work are described in Taner et al. (2021). There, accuracy is defined as:

$$Acc = \frac{TP + TN}{TP + TN + FP + FN} \tag{1}$$

where, TP is the number of true positive cases, TN is the number of true negative cases, FP is the number of false positive cases, and FN is the number of false negative cases. Moreover, precision is defined as:

$$Pr = \frac{TP}{TP + FP} \tag{2}$$

whereas, recall is defined as:

$$Re = \frac{TP}{TP + FN} \tag{3}$$

and, F1-score is defined as:

$$F1 = 2 \times \frac{Re \times Pr}{Re + Pr} \tag{4}$$

Initially, the applied architecture consisted of convolutional layers followed by max pooling layers and an output of fully connected hidden layers (Mital and Andrade, 2022). After the first trials, changes were implemented on this architecture until a final version of it was decided based on the accuracy scores given while tuning the hyperparameters (for more details of the hyperparameter tuning results, refer to Appendix). The objective of the tuning process is to get the best arquitecture for the CNN, that is, to get the best scores and reduce problems during the training process such as overfitting (i.e., the application of dropout (Srivastava et al., 2014) and batch normalization (Bjorck et al., 2018) layers help to reduce this problem).

Table 1
Parameters and output shapes of the data on each layer of the best CNN model.

Layer	Hyperparameters	Activation	Output shape
Input	41 × 41 × 41 matrix		
Conv 3D	filters: 16, kernel size: 3	TanH	39 × 39 × 39
Conv 3D	filters: 16, kernel size: 3	TanH	37 × 37 × 37
Batch Normalization			37 × 37 × 37
Max Pooling 3D	stride: 2, shape: 2 × 2 × 2		18 × 18 × 18
Conv 3D	filters: 32, kernel size: 3	TanH	16 × 16 × 16
Conv 3D	filters: 32, kernel size: 3	TanH	14 × 14 × 14
Batch Normalization			14 × 14 × 14
Max Pooling 3D	stride: 2, shape: 2 × 2 × 2		7 × 7 × 7
Flatten			10976
Dense	100 neurons	TanH	
Output		Sigmoid	1

The best model in terms of accuracy and F1-score displays a percentage of 89% correctly classified "good" grains and 90% of correctly classified "bad" grains. The architecture in Table 1 was chosen to analyze the results of the classification given by the CNN.

To better understand the classification results given by the CNN, a confusion matrix is built and shown in Fig. 9(a). This tool allows the visualization of metrics such as true positive ("good" grains correctly classified), true negative ("bad" grains correctly classified), false positive ("bad" grains classified as "good"), and false negative ("good" grains classified as "bad") cases. A higher value in precision (89%) indicates a lower rate of false positive cases (upper right value of the matrix), in contrast with a lower value of recall (85%), which indicates a higher rate of false negative cases (lower left value of the matrix).

The CNN's confusion matrix in Fig. 9(a) indicates that from a total of 300 "good" Jaramijó's digital grains, 255 (85%) were correctly classified and 45 (15%) misclassified, on the other hand, from a total

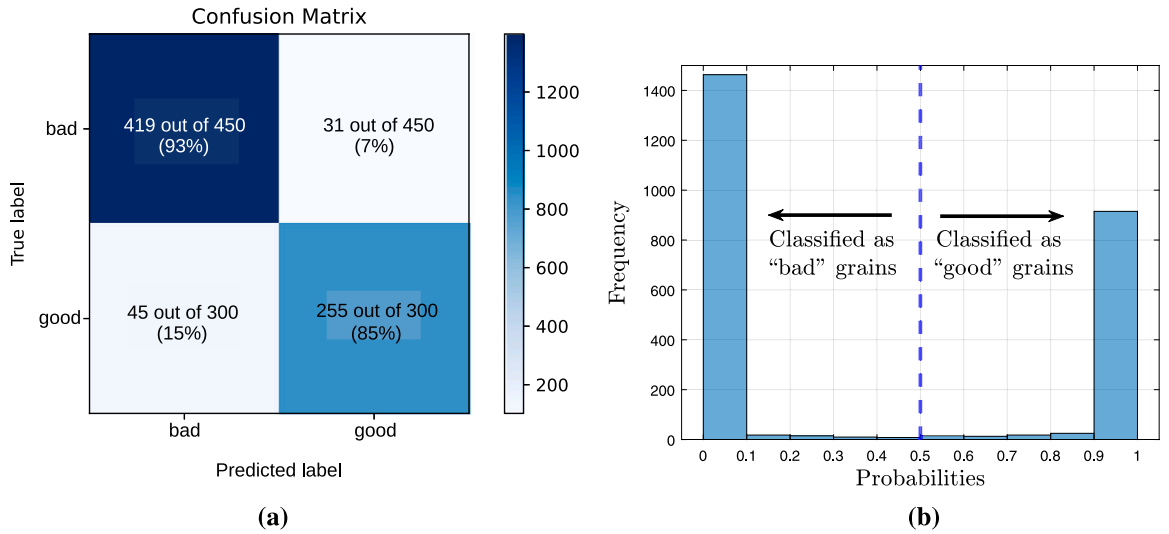

Fig. 9. Classification results of the CNN, (a) the confusion matrix indicates the values and percentages of correctly classified and misclassified grains, (b) the probability histogram is shown in order to determine the certainty in which the network classifies the grains on their respective groups, with 89% correctly classified "good" grains and 90% correctly classified "bad" grains.

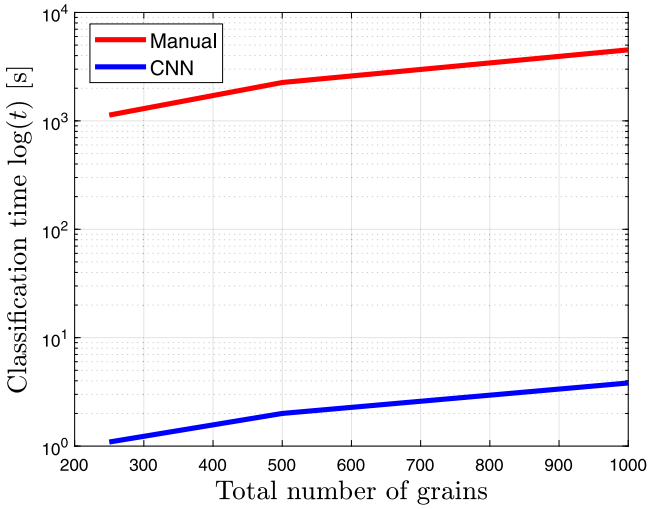

Fig. 10. Time comparison between a set of manually classified (red line) digital grains, and automatic classification by the CNN (blue line) with sets of 250, 500 and 1000 grains.

of 450 "bad" grains, 419 (93%) were correctly classified while 31 (7%) were misclassified.

In Fig. 9(b), a probability histogram of the classified digital grains is shown. The histogram visualizes the certainty of the network when it classifies each digital grain in their respective group, considering probabilities that are lower than 0.5 as "bad" grains and higher than this value as "good" grains. It is worth mentioning that the network is confident enough in the classification of the grains, existing low frequencies of probabilities between 0.1 and 0.9 and higher frequencies in range 0 to 0.1 and 0.9 to 1.

Once the CNN is trained and tested, a benchmark test was performed with the aim of estimating and comparing manual vs. CNN classification times. The test consisted of generating randomly picked groups of digital grains (250, 500 and 1000 units), each made of properly (50%) and ill-segmented (50%) grains. Then, each group was classified manually (in one seat) and with the CNN, recording the time taken for each method. The results of the test are displayed in Fig. 10.

As it can be inferred from Fig. 10, manual classification takes much more time to execute in comparison to the CNN. For a group of 250 digital grains, the estimated manual classification time is of 1129.5 s, while for the network is of 1.09 s, being the latter at least 1036 times faster. Thus, even though manual inspection of digital grains is a long, repetitive, and tedious process, it is necessary to generate a training dataset for the CNN. Nevertheless, once a couple of thousand grains are inspected and used for training, the CNN is capable of automatically distinguish a much bigger sample of digital grains in less time. For example, given a group of 200 000 digital grains, the estimated manual inspection time, based on the results in Fig. 10, would be of 903 600 s (251 h). On the other hand, to train the CNN, a group of at most 5000 grains is taken and classified in an estimated time of 6.27 h, then, the pre-processing and training estimated time is about 4 h (with the computational resources described at the start of this section), summing a total of 10.27 h. Finally, the 195 000 remaining grains are classified by the CNN in an estimated time of 12.42 minutes. Hence, the time taken to prepare the CNN until the digital grains are automatically classified is of approximately 10.5 h, which is 23.9 times faster than the manual inspection in this example.

3.2. A morphological based interpretation of the CNN's learning process

Now that a CNN architecture has been successfully trained and tested to classify the digital grains of the Jaramijó's sample, we aim to understand how the CNN is learning from the level set data used as input. For this, morphological parameters that are commonly used to describe shape qualitatively and quantitatively, such as roundness, sphericity, aspect ratio, volume, surface area, and grain's diameter, are used. The definition of the aforementioned descriptors are taken from Jerves et al. (2016), Medina and Jerves (2019) and Cho et al. (2006). For instance, sphericity is defined as:

$$S = \frac{r_{in,max}}{r_{cir,min}} \tag{5}$$

where $r_{in,max}$ is the maximum inscribable radius and $r_{cir,min}$ is the minimum circumscribable radius of a given grain. Roundness is defined as:

$$R = \frac{\frac{1}{N}\sum_{i=1}^{N} r_i}{r_{cir,min}} \tag{6}$$

where r_i is the radius of curvature at the ith corner and N is the total number of corners. Aspect ratio is defined as:

$$AR = \frac{min_{prin.-dir.}}{max_{prin.-dir.}} \tag{7}$$

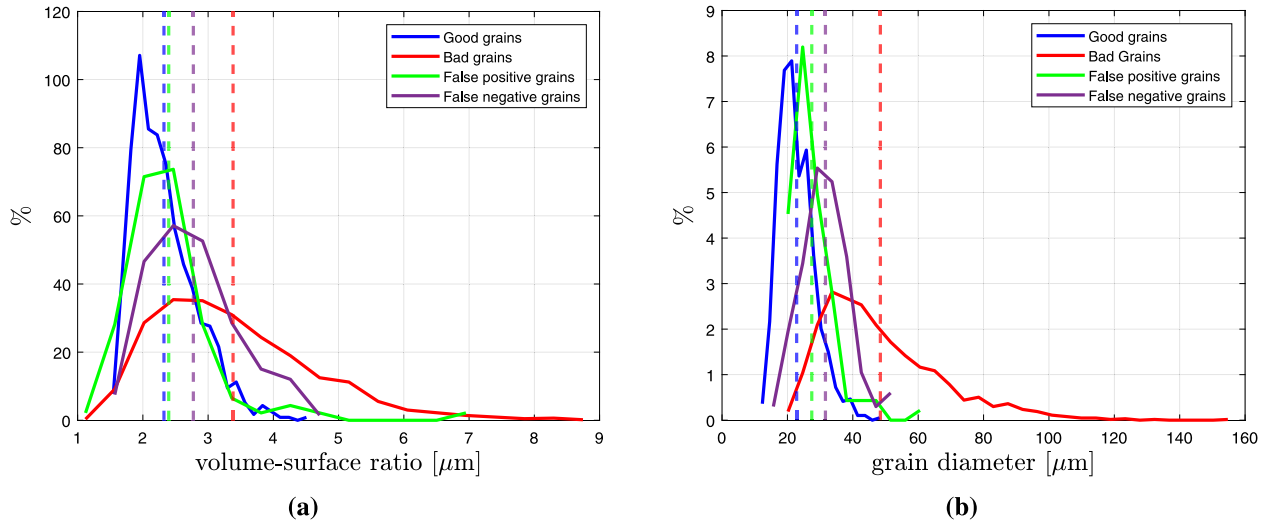

Fig. 11. Morphological distribution of the correctly classified and misclassified grains. (a) Volume-surface ratio distribution of the correctly classified and misclassified grains, (b) Diameter distribution of the correctly classified and misclassified grains.

where $min_{prin.-dir.}$ is the minimum principal direction and $max_{prin.-dir.}$ is the maximum principal direction of a given grain.

In the case of a CNN, its weights are updated during the training process, however, the specific information that the neural network is using to "learn" from the data remains unknown. In this regard, the best thing that can be done is to take an educated guess based on information from the training data that can be made sense by a person. In this section, we attempt to interpret the aforementioned learning process by using the most intuitive morphological information that can be put into quantitative and qualitative measures as described in the previous paragraph.

3.2.1. Morphological characterization of Jaramijó 's level set grains

Jaramijó's sample consists of 1500 "bad" grain level sets and 1000 "good" grain level sets, whose morphological parameters have been computed and are shown in Figs. 11 to 13.

The volume to surface ratio distributions are displayed in Fig. 11(a). The distribution of each group of digital grains ("good", "bad" and misclassified) was plotted together with their corresponding mean value. This process was repeated for all the morphological parameters considered in this study. From Fig. 11(a) it can be observed that both "good" grains and misclassified "bad" grains share similar mean values of 2.3 μm and 2.4 μm, respectively, contrasting to "bad" grains that differs with a mean value of 3.4 μm. However, misclassified "good" grains had a mean of 2.8 μm that tends to the mean of "bad" grains, being slightly off with the "good" grains' mean by 0.5 μm. In terms of volume surface ratio, some "bad" grains may be misclassified as "good" due to their similarities. Albeit, false negative grains share similar mean values between "good" and "bad", which suggests that some grains may be misleadingly classified in a wrong group.

The diameter distributions of the digital grains were plotted in Fig. 11(b). Grain's diameter is defined by the smallest sphere that contains the grain, where the sphere's diameter matches the diameter of the grain. A similar behavior as volume-surface ratio is observed, i.e., the mean values of both "good" and false positive grains (22.8 μm and 28.0 μm respectively) are comparable, contrasting with "bad" grains that have greater grain diameter values and a mean of 48 μm, which may be caused by undersegmented grains. Again, the false negative grains' mean value of 32 μm is limited between "good" and "bad" grains' diameter mean, with a difference of 9 μm and 17 μm respectively.

Aspect ratio distribution plots are shown in Fig. 12(a). In this case, a different behavior is observed, contrasting with the digital grains' diameter and volume to surface ratio plots. For "good" grains, aspect ratio have a slightly higher mean value (0.62) in comparison to the mean of "bad" grains (0.56), and both false negative, and false positive grains (0.57) are close to the aspect ratio mean of "bad" grains. In terms of aspect ratio, the distribution plots are similar, i.e., there is little difference between the mean value of each group. This suggests that the CNN may have difficulties to differentiate the grains based solely on aspect ratio.

Sphericity's morphological distribution is plotted for each group in Fig. 12(b). A clear difference between "good" and "bad" grains is noted, with means of 0.33 and 0.27, respectively. The mean value of misclassified grains tends to move to the mean value of "bad" grains, with both false negative, and false positive grains with almost identical mean sphericity (0.29). This may indicate that the network could correctly classify digital grains with bigger values of sphericity, in comparison to grains with smaller sphericity values.

Finally, a plot of roundness distribution, seen in Fig. 13, is analyzed. The first observation is the difference between "good" and "bad" digital grains, with means of 0.90 and 0.73 respectively. Then, once more, false negative and false positive grains share similar mean values with 0.85 and 0.86 respectively. Thus, in terms of roundness the network could correctly identify "bad" grains with lower roundness than "good" grains. Nevertheless, in both groups there were grains with similar roundness values, in which the network had difficulties to differentiate, thus including them in their wrong group.

Almost every distribution has similar behavior, with exception of volume-surface ratio seen in Fig. 12(a) were false positive grains had a similar mean than "good" grains. Fig. 14 displays a group of misclassified grains, both false positive and false negatives, with slightly difficult errors to spot or possible patterns in the morphology that could cause confusion to the CNN, with their corresponding mean value in each morphological parameter in which it is observed that in most cases are similar between each other.

Mean measures of Jaramijó's digital "good", "bad", false positive and false negative grains were calculated in Table 2.

4. CNN-based classification of other digitalized soil samples

4.1. Martian Regolith Simulant sample (sensibility testing)

Once the CNN is trained and tested with Jaramijó's level set-based grain representations, yielding an accuracy of up to 90%, a sensibility test is performed with another soil sample to estimate the dependency

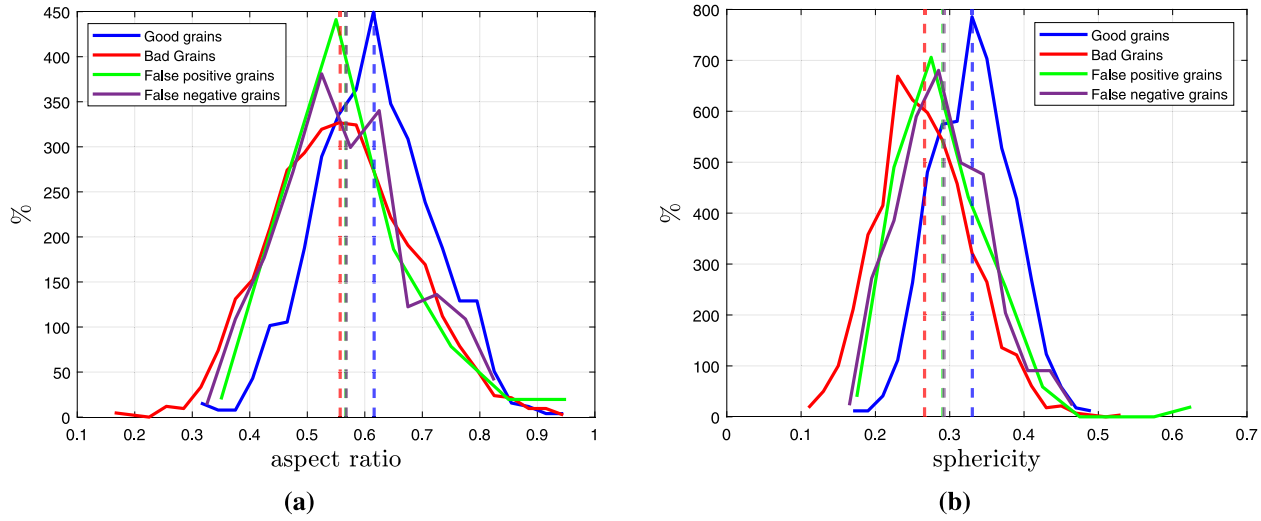

Fig. 12. Morphological distribution of the correctly classified and misclassified grains. (a) Aspect ratio distribution of the correctly classified and misclassified grains. (b) Sphericity distribution of the correctly classified and misclassified grains.

Table 2
Mean values of Jaramijó's classified digital grains.

Parameter	"good" grains	"bad" grains	False negative grains	False positive grains
Roundness	0.90	0.73	0.85	0.86
Sphericity	0.33	0.27	0.29	0.29
Diameter	23	48	32	28
Aspect Ratio	0.62	0.56	0.57	0.57
Volume surface ratio	2.3	3.4	2.8	2.4

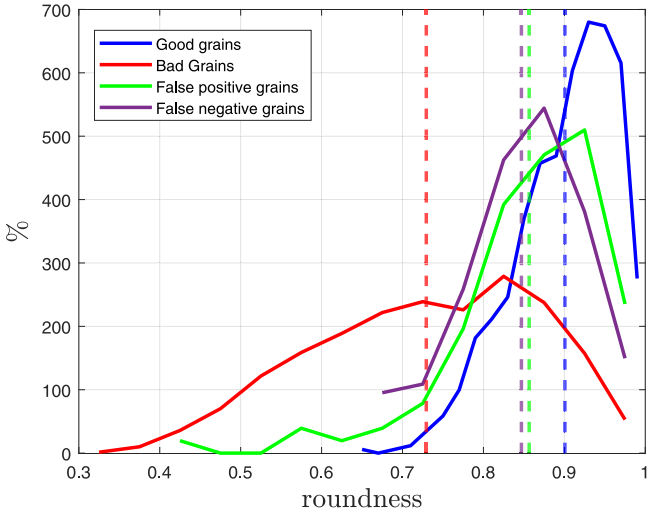

Fig. 13. Roundness distribution of the correctly classified and misclassified grains.

of the CNN on the type of granular material. With this purpose, a dataset of 2000 previously segmented and manually inspected "good" level set-based Martian Regolith Simulant grains is used (raw 3DXRCT images are not available). The dataset is pre-processed, following the procedure described in Section 3.1, and then classified by the CNN. Its performance is shown by the probability histogram of Fig. 15.

The histogram of Fig. 15 shows that the CNN trained with Jaramijó's digital grains failed to correctly identify Regolith simulant "good" grains. Just the 6% of grains are being classified correctly, indicating that the actual CNN model just works to classify Jaramijó's digital grains and is unable to properly classify other granular material.

4.2. Øysand and Hostun sand samples

The incorrect classification of Martian Regolith Simulant's digital grains demonstrates that there is a need to retrain the CNN with information specific to the granular material of interest. For that purpose, raw 3DXRCT images from samples of Øysand (2000 × 2000 × 2000 voxel) and Hostun sand (1500 × 1500 × 1500 voxel) (see Fig. 16) are processed using the algorithm described in Fig. 4.

Once the raw 3DXRCT images from Øysand and Hostun sand are processed, each one of the grains' level set representation is manually inspected. Then, for each sample, the cumulative grain size distribution from the properly segmented digital grains is obtained and validated with respect to its counterpart from the physical laboratory, as shown in Fig. 17.

A similar analysis to the one performed for Fig. 7, in Section 2.2, is carried out for Fig. 17(a). Here, the level set-based Øysand grains give a $C_u = 1.41$ and a $C_c = 0.98$, that are comparable to the values yielded by their real counterparts, i.e., $C_u = 1.47$ and $C_c = 0.97$. Thus, note that C_c is almost the same for the digital and real samples, error = 1.21%, while for C_u the error is of 3.83%. In terms of size and statistical convergence, the digital sample made of 604 grains, corresponds to nearly 50% of the real sample (1442 grains). Hence, the digital sample grain size distribution shows physical as well as statistical convergence (see Fig. 17(a)).

Additionally, the Hostun digital sample (see Fig. 17(b)) displays a $C_u = 1.33$ and a $C_c = 0.99$, that show convergence to the $C_u = 1.42$ and $C_c = 0.96$ from the real sample. In this case, the error is of 3.76% and 6.51%, respectively. Finally, in terms of statistical significance, the digital sample is composed of 8497 grains.

Finally, the level set-based grains are labeled and pre-processed to separate 70% of the grains for training, and 30% left for testing the CNN. With an existing pre-trained CNN model, a training method defined as Transfer Learning could be considered instead of training the

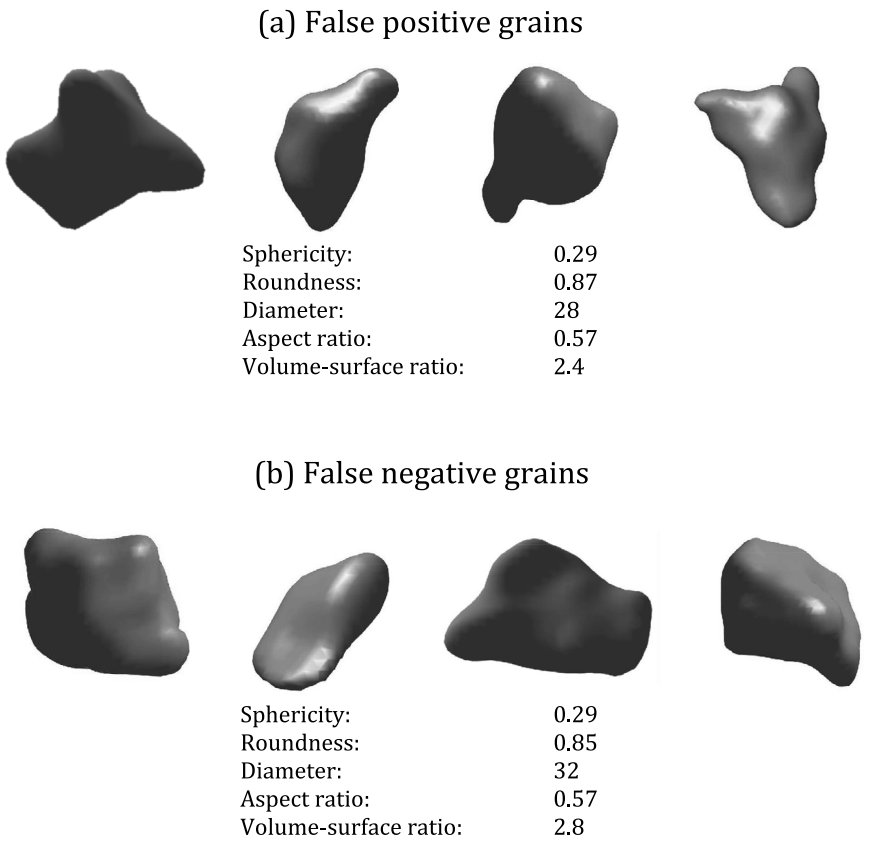

Fig. 14. Morphological comparison between (a) misclassified digital "bad" grains (top row) and (b) misclassified "good" grains (bottom row), with their means on their respective morphological parameter.

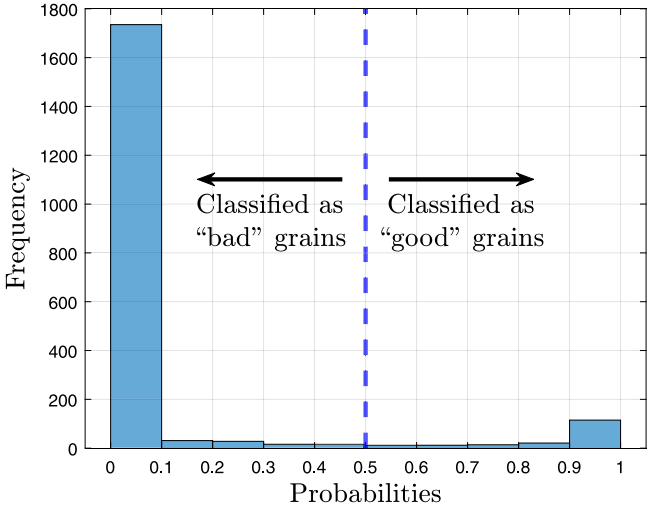

Fig. 15. Probability histogram of the CNN tested on 2000 "good" Martian Regolith Simulant digital grains, with only 6% of grains correctly classified as "good".

CNN from scratch. Transfer learning consists of freezing the weights of a previously trained CNN model, eliminating only the last fully connected layers and replacing them with new ones, whose weights are updated with the new input data during the training process (Tammina, 2021; Lu et al., 2015; Brownlee, 2019; Chollet, 2020). It is worth mentioning that transfer learning have advantages such as fast training, reaching the highest classification accuracy in less epochs. Thus, it allows to use a small data set as input. However, in case of overfitting, early layers cannot be modified as an attempt to solve it, being a disadvantage for transfer learning.

In the following subsections, the selected CNN model is trained from scratch and with transfer learning using digital grains from Øysand and Hostun sand, with the objective to compare which method is adequate for this particular classification task (classification between "faithful" and ill-segmented digital grain representations), evaluating the results of each method with the same metrics described in Section 3.1.

Remark

Applying the most optimal parameter tuning to the algorithm described in Fig. 4, a 3DXRCT scan from an Øysand sample was processed. Thus, a total of 1350 digital grains was obtained, with 987 (73.11%) "good" and 363 (26.89%) "bad" grains. However, the image processing results of the same Øysand sample introduced in the following section corresponds to a non optimal set of parameters applied to Fig. 4. This was performed with the aim of obtaining a greater amount of "bad" grains, so the CNN can be trained in a more proper manner.

4.2.1. Øysand

For Øysand fine gravel, a total of 1405 digital grains were used, a sample of 4 out of 604 "good" and 4 out of 801 "bad" grains are displayed in Fig. 18.

With the manually inspected digital grains, the data is pre-processed and used as input for the CNN. A total of 983 grains were used for training and 422 for testing. Transfer learning gave better results in terms of accuracy (84%), in comparison with training from scratch (83% of accuracy). The classification results were analyzed with the aid of the confusion matrix (see Fig. 19) for transfer learning method.

With the results shown by the confusion matrix of Fig. 19. It is inferred that the base model of the CNN can be successfully trained with

Fig. 16. Sample of (a) Hostun sand and (b) Øysand.

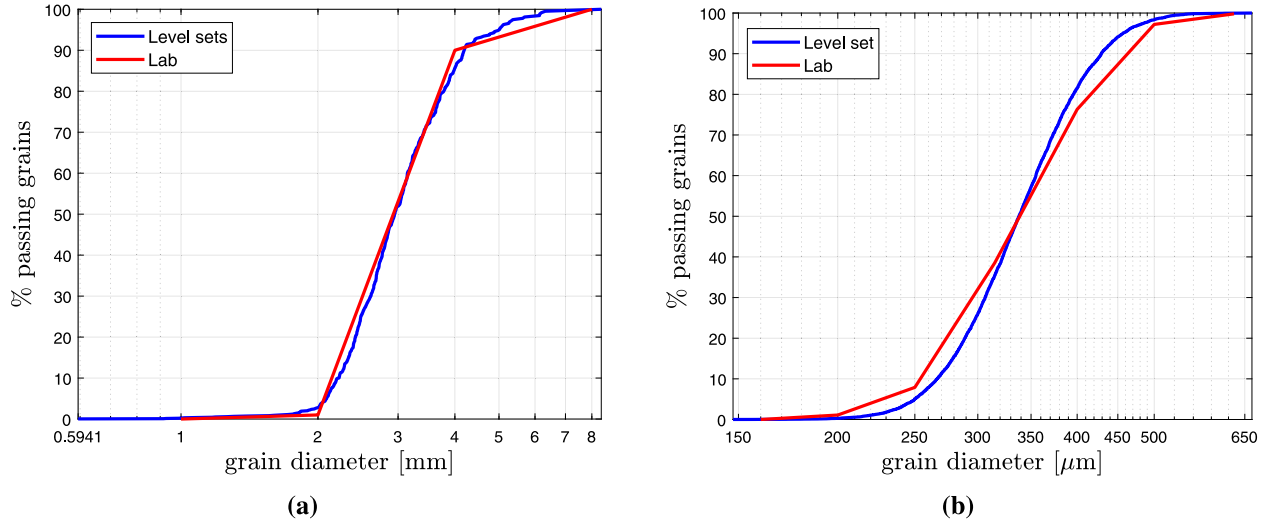

Fig. 17. Grain size distribution of (a) 604 Øysand grains and (b) 8497 Hostun sand grains. Digital grains (blue line), and physical laboratory results (red line).

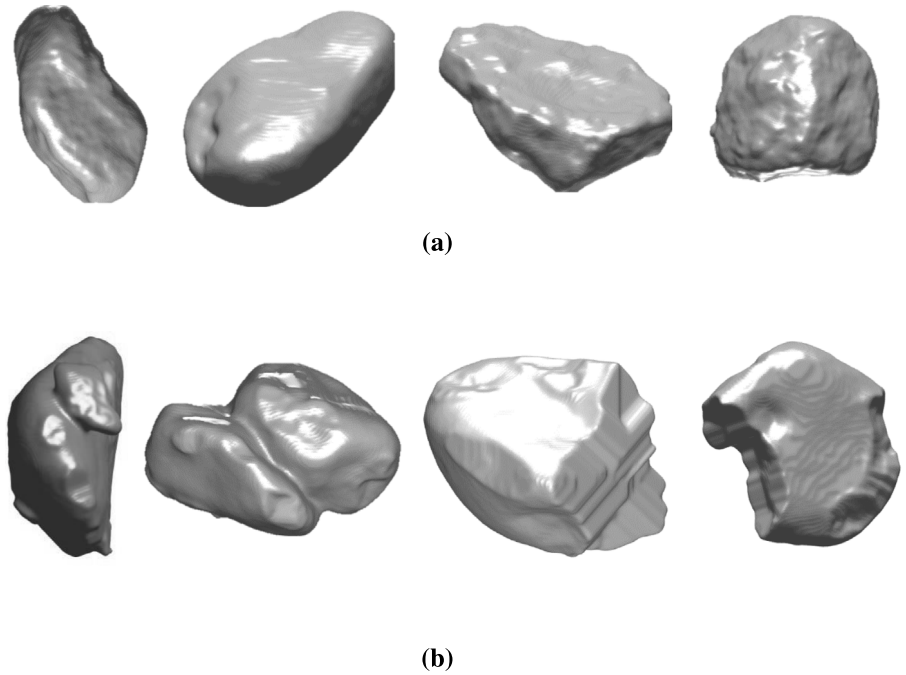

Fig. 18. Examples of processed (a) "good" grains and (b) "bad" grains from Øysand soil.

Table 3
Mean measures of Øysand's classified grains.

Parameter	"good" grains	"bad" grains	False negative grains	False positive grains
Roundness	0.17	0.17	0.17	0.17
Sphericity	0.43	0.38	0.42	0.39
Diameter	2.91	3.27	3.05	3.36
Aspect Ratio	0.54	0.53	0.55	0.54
Volume surface ratio	0.55	0.53	0.56	0.54

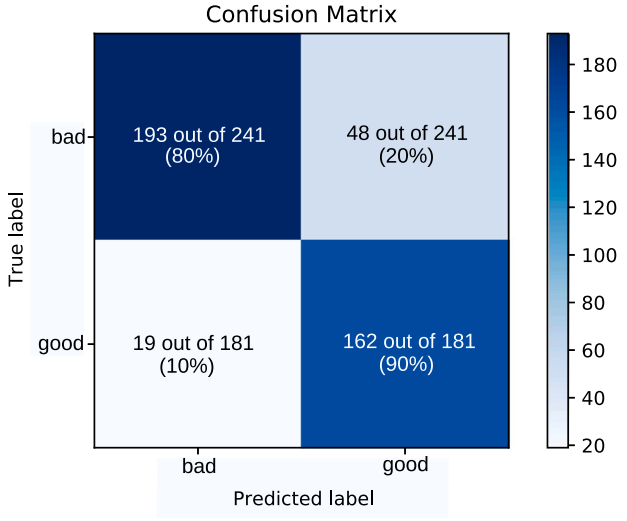

Fig. 19. Classification results of the CNN trained with Øysand grains using transfer learning.

information from other granular materials. In this case, the confusion matrix displays an asymmetry, suggesting a better classification ratio of "good" grains (grains predicted as "good" actually belong to that group).

Similarly than with the soil sample from Jaramijó, the morphological parameters of the classified digital grains are analyzed, grouping the mean value of each parameter in Table 3.

From Table 3, note that "good" and "bad" digital grains have similar mean values. Also, the mean values of misclassified grains do not show significant difference either. This suggests that it was challenging for the CNN to distinguish patterns, in terms of morphological parameters, between each group of grains. Moreover, this might also explain the lower classification accuracy (84%) for Øysand in comparison to the accuracy of the CNN trained with Jaramijó's digital grains (90%).

4.2.2. Hostun sand

A group of 3325 Hostun sand digital grains were obtained following the steps from Fig. 4. A sample of 4 out of 2040 "good" and 4 out of 1285 "bad" Hostun digital grains are displayed in Fig. 20.

After pre-processing the data, the CNN is trained with the Hostun sand digital grains. A total of 2327 digital grains were used for training and 998 for testing. In this case, training from scratch gave better results in terms of accuracy (84%), when compared to transfer learning (82% of accuracy). Similarly as with Øysand, the classification results are analyzed with the confusion matrix in Fig. 21. This yields an asymmetry, in the same way, the recall obtained is higher than the precision, with 90% and 86% respectively.

For Hostun sand, the CNN trained from scratch could be tested on more unknown data. Besides from the group of 3325 manually inspected digital grains, another group of 12188 grains was processed, using the CNN to classify them. It is worth noticing that while the estimated manual inspection time taken to prepare the dataset of 3325 digital grains for training was of 4.17 h, the remaining 12188 grains were classified by the CNN in an estimated time of 53 s, observing the potential scope of this tool. The CNN identified a total of 7718 "good" grains and 4470 "bad" grains. Then, the 7718 classified as "good" grains were manually inspected, for testing purposes, to determine what percentage of grains actually belonged to that group. From the group of 7718 classified as "good" digital grains, 6468 were actually "good" and 1250 were misclassified, which represents a classification accuracy of 84%.

From a group of both manually and CNN classified grains, a total number of 8497 Hostun sand digital grains were obtained. As an attempt to reconstruct the original sample in 3D (see Fig. 22), the centroid of each grain was calculated, locating them in their corresponding position.

In the render of Fig. 22, some blank spaces may be spotted between the grains, corresponding to the "bad" grains that were not included in the reconstruction of the sample. In general, missing grains do not represent an issue to characterize the mechanical behavior of the sample, only the right morphology is required. When a bigger size of the sample is needed, "bad" grains may be compensated with a cloning algorithm (Medina and Jerves, 2019) that increases the amount of grains while maintaining the morphological parameters of the sample.

Sometimes, to characterize granular material at a microscopic scale, the reconstruction of the whole original sample may be required to simulate experiments, like the triaxial test that tracks the evolution and interaction of each grain in a real soil sample (such as the studies carried out by Andò et al., 2012; Cheng and Wang, 2018). Our approach makes it possible to locate each "bad" digital grain in the tomography and reprocess it, as shown in Fig. 23, with the objective to reconstruct a one to one digital representation of the original sample.

Finally, an analysis on morphological parameters of Hostun sand's digital grains was made. Reviewing the morphological parameters distributions, it can be inferred that Hostun sand results are comparable with the results from Øysand. Both have similar distributions corresponding to each group of grains ("good", "bad", false positive and false negative grains), and their corresponding mean values are similar between each other, indicating that there is not much difference in morphological parameters when contrasting "good" with "bad" grains. Hence, the CNN faced a challenge at the time of classification. The mean measures of the described and analyzed morphological distributions were grouped in Table 4.

4.2.3. Transfer learning vs. training from scratch

In sub- Sections 4.2.1 and 4.2.2 only the best training results were displayed. Training from scratch and transfer learning yield similar classification results, with a maximum difference of 2% in accuracy and 1% in F1-score. Thus, not particular method was proved to be the best.

As a second evaluation criteria, the number of epochs taken to reach the maximum classification accuracy during training (with each method) was analyzed, also studying the influence of the number of digital grains used for training the CNN. For this purpose, a test was carried out as follows: from the total number of Øysand and Hostun sand digital grains (1405 and 3325 respectively), random sub-datasets of 250, 500 and 1000 grains were made for each soil sample. The same ratio between "good" and "bad" grains (43% "good" and 57% "bad" for Øysand, and 61% "good" and 39% "bad" for Hostun sand) is kept. Then, each dataset is used to train the CNN with transfer learning and learning from scratch, determining the classification accuracy and number of epochs taken. The results of this test are shown in Fig. 24.

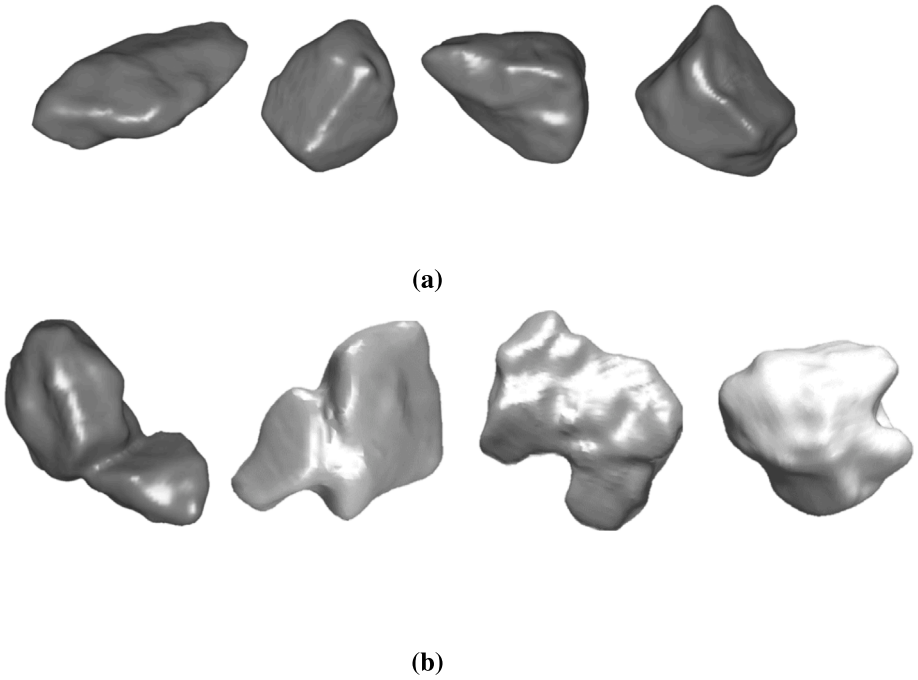

Fig. 20. Examples of processed (a) "good" grains and (b) "bad" grains from Hostun sand.

Table 4
Mean measures of Hostun classified grains.

Parameter	"good" grains	"bad" grains	False negative grains	False positive grains
Roundness	0.54	0.51	0.53	0.55
Sphericity	0.39	0.34	0.37	0.38
Diameter	0.52	0.66	0.57	0.60
Aspect Ratio	0.56	0.55	0.56	0.57
Volume surface ratio	0.055	0.058	0.056	0.054

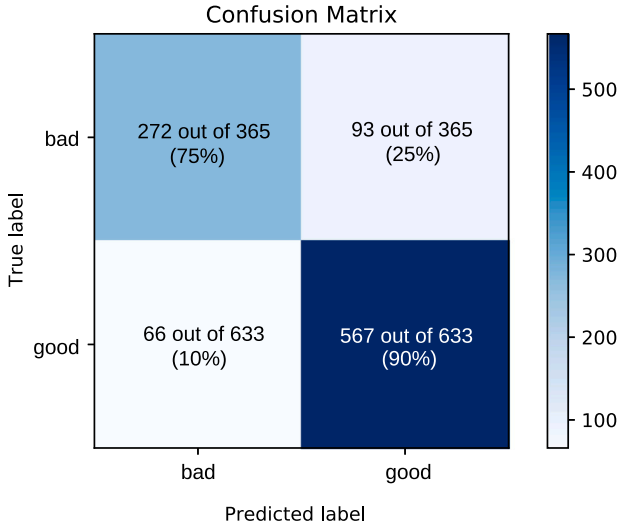

Fig. 21. Classification results of the CNN trained from scratch using Hostun sand grains.

In Fig. 24(a) it is observed that, for Øysand, a better accuracy is obtained with transfer learning in comparison with training from scratch. On the other hand, with Hostun sand in Fig. 24(b), training from scratch gave better accuracy than transfer learning. However, the difference in accuracy between each method is of 3% maximum, which does not represent a significant difference when classifying the grains. From the results of Fig. 24, it is determined that either method may be appropriate to train other granular materials. The main advantage of transfer learning over training from scratch is a smaller number of epochs required to reach the maximum accuracy, as seen in Fig. 24, which represents a lower computational cost at the time of training the network.

5. Further improvements

The image processing algorithm can be further improved in order to obtain more digital avatars of grains from raw 3DXRCT images. In the present work, one of the steps that takes time to apply on the 3DXRCT images and demands high costs of computational resources is the non-local means filter. In future works, the non-local means filter, and other steps in the algorithm, could be optimized with high-performance computing (HPC) parallelization techniques, thus taking advantage of a multiprocessor system to execute several instructions at the same time, speeding up the processing time of the algorithm.

Further work can be done in order to reduce under and over-segmentation of the image processing algorithm. In some cases, tiny local minima filtering helps to reduce the amount of grains that were being oversegmented. Yet, as stated before, its parameters still need to be calibrated depending on the granular material and the quality of the CT scan (voxel size, noise, composition of material, etc.). Also, other watershed techniques, such as marker based or adaptive watershed, could be tested and evaluated. A neural network approach trained to identify contacts between grains may also help to overcome segmentation problems of the image processing.

The centroid calculation of each individual grain allows us to locate them in the 3DXRCT image, that includes both "good" and "bad" digital grains. With this approach, in case that a one to one representation

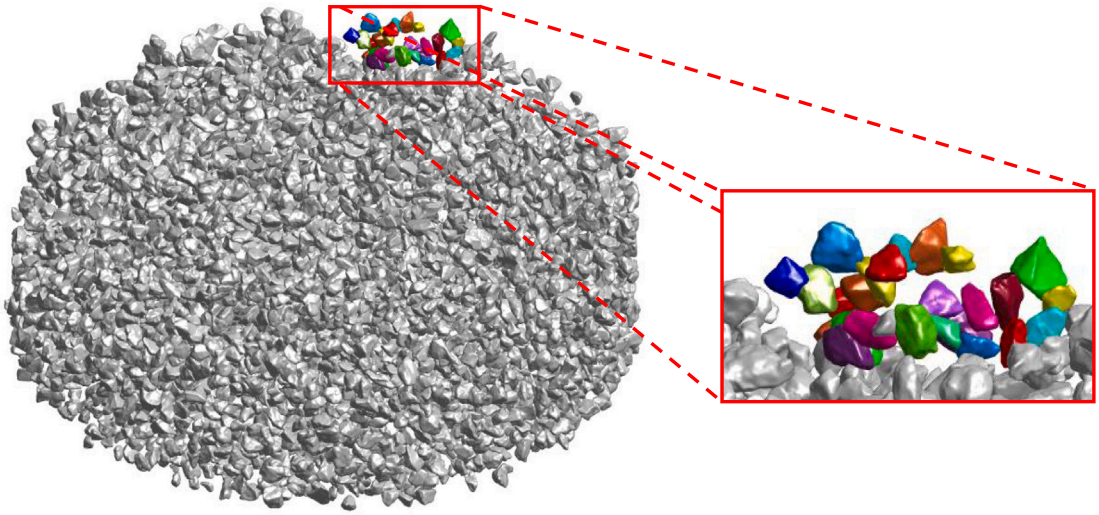

Fig. 22. 3D render of the Hostun sand sample consisting of 8497 "good" grains and their respective original positions obtained as in the laboratory from the image processing algorithm.

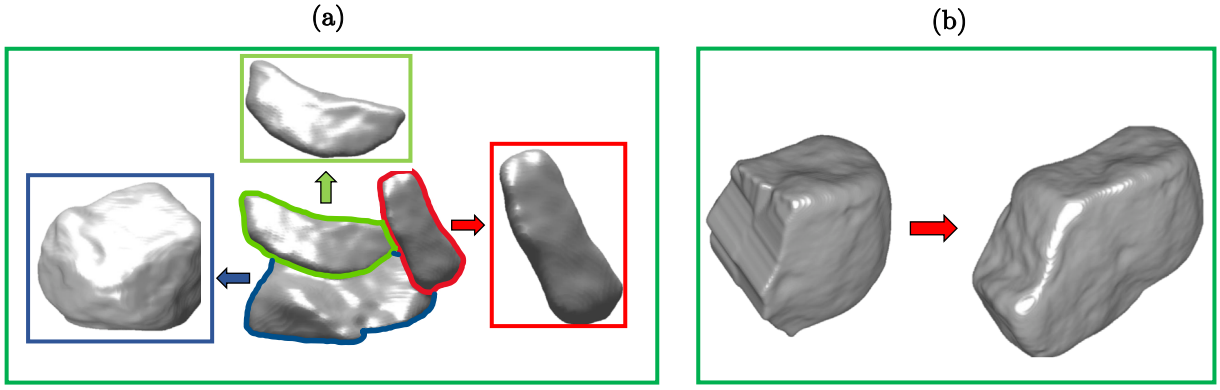

Fig. 23. Reprocessed "bad" grains. (a) A case of undersegmentation where the joined grains were successfully separated. (b) A case of oversegmentation where the whole grain could be obtained.

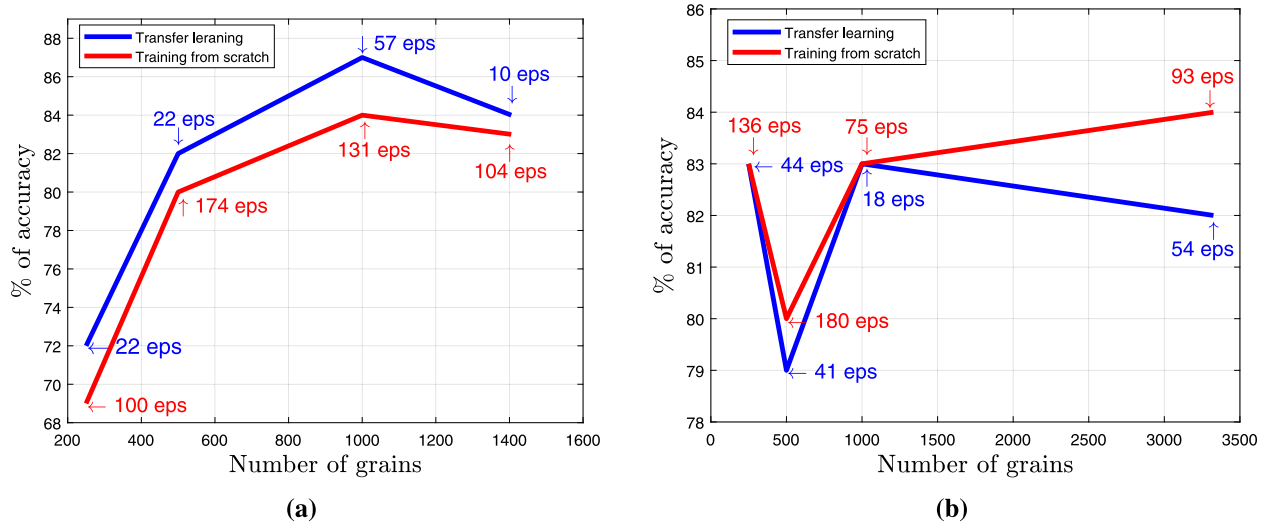

Fig. 24. Accuracy vs number of grains used to train the CNN with transfer learning and training from scratch, and the corresponding number of epochs (eps) using: (a) random sub-datasets of Øysand grains and (b) random sub-datasets of Hostun sand grains.

of the original sample is needed, the group of "bad" digital grains can be reprocessed, securing to correct every segmentation error.

The digital grains classified as "good" by the CNN were used in 3DLS-DEM-based simulations. While the results of the simulations were being evaluated, it was noted that some grains had an inconsistent behavior, yielding incorrect results. This group correspond to misclassified grains that went "under the radar", being an error that also happens in manual inspection, induced by inherent human error. However, the CNN can always be further improved to reach a higher classification accuracy, reducing the number of misclassified grains for 3DLS-DEM-based virtual laboratory experiments. Some improvements include a different model with its respective hyperparameter tuning, or to increase the amount of "good" and "bad" digital grains as training data. Finally, it is worth pointing out that most "bad" grains that are misclassified by the algorithm as "good", come from undersegmentation in the image processing.

At this point, all of the image processing algorithm and the input data pre-processing for the CNN are implemented in Matlab, and the CNN's training and prediction are implemented in Python. In the future, we aim to establish a single pipeline for all these processes, starting from the import of a sample's raw 3DXRCT image, until the classification of the obtained digital grains between "good" or "bad".

6. Conclusion

In the present work we have introduced a new tool to speed up the digitalization process of grains from a raw 3DXRCT image of a sample, involving a CNN in the process. The digital grains are obtained with an image processing algorithm that generates a level set representation of each grain, which needs to be manually inspected, one by one, to discard incorrectly segmented grains. This tool implements a CNN (trained with Jaramijó's soil level set digital grain representations as ground-truth) that classifies the digital grains between "faithful" or ill-segmented representations with a validation accuracy above 80%, speeding up the manual inspection process by at least 1036 times.

The tool is general enough to be applied in natural and artificially modified granular materials, with techniques such as training from scratch or transfer learning. Training from scratch is a common process when a same architecture is used to do a different task, in contrast, transfer learning uses an already trained architecture and adapts it to solve other problem with similar features. Both methods were tested with manually classified digital grains of Hostun sand and Øysand, using as a base model the architecture trained with Jaramijó's soil digital grains for transfer learning. In general, neither training from scratch nor transfer learning provided any significant difference, both methods can be used when training the CNN with other granular material. However, transfer learning takes less epochs to reach the maximum classification accuracy, representing a lower computational cost during training, while providing similar results when compared to training from scratch.

To obtain more "faithful" segmented digital grains from a raw 3DXRCT image, four improvements were implemented in the image processing algorithm. First, a calibrated CLAHE filter was applied to the raw 3DXRCT image to improve its contrast, helping in later binarization process. Second, a filling algorithm was implemented to fix the holes inside some grains in the binarized image. Third, as a solution for some over segmented grains, tiny local minima filtering with extended minima transform is used as part of the watershed segmentation process. And fourth, with the labeled image obtained from the watershed algorithm, the centroid of each grain in the 3DXRCT is calculated, allowing to locate and reprocess them if needed.

All of the image processing algorithm is implemented following a single pipeline, i.e., every step of the algorithm is implemented in Matlab using its built-in functions, starting from the import of a 3DXRCT image, to the generation of the level set representation of each individual grain in the 3DXRCT image.

The developed tool generates digital grain avatars (one to one representation) from natural or artificial soil samples, towards the creation of an automated and industrialized 3DLS-DEM-based virtual laboratory pipeline (a one-stop shop). Thus, these avatars can be used for an accurate 3D morphological as well as physical characterization via 3DLS-DEM-based virtual laboratory testing. Finally, this pipeline not only enables the creation of databases of digitalized soil samples from around the world together with their phenomenological, state, and morphological parameters. Most of all, it allows for the design and testing of new novel granular materials and their potential applications.

CRediT authorship contribution statement

Stefano Buitrón Cevallos: Software, Validation, Formal analysis, Investigation, Data curation, Writing – original draft, Writing – review & editing, Visualization. **Alex X. Jerves:** Conceptualization, Methodology, Software, Validation, Formal analysis, Investigation, Resources, Data curation, Writing – original draft, Writing – review & editing, Visualization, Supervision, Project administration, Funding acquisition. **Utkarsh Mital:** Conceptualization, Methodology, Software, Validation, Formal analysis, Investigation, Data curation, Writing – review & editing. **David A. Medina:** Investigation, Writing – original draft, Writing – review & editing. **V. Santiago Quinteros:** Resources, Writing – review & editing. **Maurizio Mulas:** Investigation, Resources. **Øyvind Torgersrud:** Resources, Writing – review & editing.

Declaration of competing interest

The authors declare that they have no known competing financial interests or personal relationships that could have appeared to influence the work reported in this paper.

Data availability

Data will be made available on request.

Acknowledgment

The CNN was developed and tested using the free cloud services hosted by Google Colab. The Hostun sand's image was provided by Prof. Edward Andò from EPFL, Switzerland.

Appendix

Image processing algorithm calibration

Some parameters from the image processing algorithm, displayed in Fig. 4, are calibrated depending on the soil sample. In the following table, the respective parameters used for Jaramijó's sand, Øysand and Hostun sand are specified. It is worth noticing that the parameters in Fig. 4 that are not included in the table are the same for all the soil samples (see Table A.1).

Table A.1
Image processing algorithm parameters calibrated depending on the soil type.

Filter:	Tiny local minima	NLM	CLAHE
Parameter:	H-minima	Filter strength	Clip limit
Jaramijó	1	0.11	0.005
Øysand	2	0.04	0.01
Hostun sand	2	0.09	0.005

Table A.2
Parameters of the different tested CNNs models.

Parameters	Models			
	Sigmoid 1	Sigmoid 2	Sigmoid 3	TanH
Convolutions	2	4	5	4
Activation function	Sigmoid	Sigmoid	Sigmoid	TanH
Filters	10–20	16–16–32–32	10–10–20–20–40	16–16–32–32
Kernel Size	5–5	5–5–5–5	5–5–5–5–3	3–3–3–3
Dropout	0	0	0.1	0
Batch normalization	Yes	No	Yes	Yes
MaxPooling	2 × 2 × 2	2 × 2 × 2	2 × 2 × 2	2 × 2 × 2

Table A.3
Metrics of the different trained CNNs and their percentages of correctly classified grains.

Model	Precision	Recall	Accuracy	F1 Score	Correctly Classified	
					"good" grains	"bad" grains
Sigmoid 1	90%	83%	89%	86%	90%	88%
Sigmoid 2	76%	88%	86%	81%	76%	93%
Sigmoid 3	74%	90%	86%	81%	74%	95%
TanH	84%	90%	90%	87%	90%	89%

Hyperparameter tuning

This method is known as hyperparameter tuning (Lianne, 2020), it establishes a range of, or, certain values which will be evaluated on some training epochs, then the best results are taken and the model is then trained again, with more epochs if necessary, to evaluate the results. In the following table, four evaluated and tuned architectures are listed including filter number, activation functions, kernel sizes, dropout and application of batch normalization used (see Table A.2).

The evaluation criteria consisted of the analysis of prediction of data based on accuracy. However, since the data is unbalanced (more "bad" than "good" grains) this metric not necessarily gives a correct estimation of the performance. Instead, it is possible to analyze other metrics such as precision (of all positive predictions, how many were correct) and recall (of all the positive cases in the dataset, how many were predicted correctly). In the following table, the metrics for the architectures tried (see previous table), are presented, including the percentages of correctly classified "good" and "bad" grains, and a F1-score metric, which computes both precision and recall to give a general overview of the performance of the neural network (see Table A.3).

References

Aksu, G., Oktay, C., Taha, M., 2019. The effect of the normalization method used in different sample sizes on the success of artificial neural network model. Int. J. Assess. Tools Educ. 6 (2), 170–192, https://doi.org/10.21449/ijate.479404.

Andò, E., Hall, S., Viggiani, G., Desrues, J., Bésuelle, P., 2012. Experimental micromechanics: grain-scale observation of sand deformation. Géotech. Lett. 2 (3), 107–112. http://dx.doi.org/10.1680/geolett.12.00027.

Andò, E., Viggiani, G., Hall, S.A., Desrues, J., 2013. Experimental micro-mechanics of granular media studied by x-ray tomography: recent results and challenges. Géotech. Lett 3 (3), 142–146. http://dx.doi.org/10.1680/geolett.13.00036.

Bjorck, J., Gomes, C., Selman, B., Weinberger, K.Q., 2018. Understanding batch normalization. In arXiv [cs.LG]. https://proceedings.neurips.cc/paper/2018/file/36072923bfc3cf47745d704feb489480-paper.pdf.

Bradley, D., Roth, G., 2007. Adaptive thresholding using the integral image. J. Graph. Tools 12 (2), 13–21. http://dx.doi.org/10.1080/2151237x.2007.10129236.

Brownlee, J., 2019. Transfer learning in keras with computer vision models. Machine Learning Mastery. https://machinelearningmastery.com/how-to-use-transfer-learning-when-developing-convolutional-neural-network-models/ (Accessed 24 September 2021).

Burney, A., Syed, T.Q., 2016. Crowd video classification using convolutional neural networks. Int. Conf. Front. Inform. Technol. (FIT) 24, 7–251. http://dx.doi.org/10.1109/FIT.2016.052.

Bustamante, D., Jerves, A.X., Pazmiño, S.A., 2020. A generalized three-dimensional discrete element method with electrostatic induced cohesion. Gran. Matter 22 (4), http://dx.doi.org/10.1007/s10035-020-01048-4.

Cheng, Z., Wang, J., 2018. Experimental investigation of inter-particle contact evolution of sheared granular materials using X-ray micro-tomography. Soils Found. 58 (6), 1492–1510. http://dx.doi.org/10.1016/j.sandf.2018.08.008.

Cho, G.C., Dodds, J., Santamarina, J.C., 2006. Particle shape effects on packing density, stiffness, and strength: Natural and crushed sands. J. Geotech. Geoenviron. Eng. 132 (5), 591–602. http://dx.doi.org/10.1061/(asce)1090-0241(2006)132:5(591).

Chollet, F., 2020. Transfer learning & fine-tuning. Keras.Io. https://keras.io/guides/transfer_learning/ (Accesed 24 September 2021).

CompareNetworks, 2009. Particle size analyzer (particle analyzers/particle sizer). Labcompare. https://www.labcompare.com/laboratory-analytical-instruments/32-particle-size-analyzer-particle-analyzers-particle-sizer/ (Accessed 23 November 2022).

Daub, E.G., Manning, M.L., Carlson, J.M., 2010. Pulse-like, crack-like, and supershear earthquake ruptures with shear strain localization. J. Geophys. Res. 115 (B5), http://dx.doi.org/10.1029/2009jb006388.

Digabel, H., Lantuejoul, C., 1978. Iterative algorithms. In: Proceedings of 2nd European Symposium on Quantitative Analysis of Microstructures in Material Science, vol. 8. pp. 5–99.

Dill, V., Franco, A.R., Pinho, M.S., 2015. Automated methods for hippocampus segmentation: the evolution and a review of the state of the art. Neuroinform 13, 133–150. http://dx.doi.org/10.1007/s12021-014-9243-4.

Guo, T., Dong, J., Li, H., Gao, Y., 2017. Simple convolutional neural network on image classification. In: 2nd International Conference on Big Data Analysis (ICBDA), vol. 72. pp. 1–724. http://dx.doi.org/10.1109/ICBDA.2017.8078730.

Jerves, A., Ávila, C., Mulas, M., Galindo Torres, S., Samaniego, E., 2019. Across fields and scales: an integrating roadmap for the prediction and prevention of volcanic lahar phenomena. Adv. Eng. Res. Retrieved June 11, 2022, from https://novapublishers.com/shop/advances-in-engineering-research-volume-32/.

Jerves, A.X., Kawamoto, R.Y., Andrade, J.E., 2016. Effects of grain morphology on critical state: a computational analysis. Acta Geotech. 11 (3), 493–503. http://dx.doi.org/10.1007/s11440-015-0422-8.

Juba, B., Le, H.S., 2019. Precision-recall versus accuracy and the role of large data sets. In: Proceedings of the AAAI Conference on Artificial Intelligence, vol. 33. (01), pp. 4039–4048. http://dx.doi.org/10.1609/aaai.v33i01.33014039.

Kawamoto, R., Andò, E., Viggiani, G., Andrade, J.E., 2016. Level set discrete element method for three-dimensional computations with triaxial case study. J. Mech. Phys. Solids 91, 1–13. http://dx.doi.org/10.1016/j.jmps.2016.02.021.

Khandelwal, R., 2020. Convolutional neural network: Feature map and filter visualization. Towards Data Science. https://towardsdatascience.com/convolutional-neural-network-feature-map-and-filter-visualization-f75012a5a49c (Accessed 20 March 2021).

Kim, M., Wu, G., Shen, D., 2013. Unsupervised deep learning for hippocampus segmentation in 7.0 Tesla MR images. In: Wu, G., Zhang, D., Shen, D., Yan, P., Suzuki, K., Wang, F. (Eds.), Machine Learning in Medical Imaging, MLMI. In: Lecture Notes in Computer Science, vol. 8184, Springer, Cham, pp. 1–8. http://dx.doi.org/10.1007/978-3-319-02267-3_1.

Kim, Y., Yun, T.S., 2021. How to classify sand types: A deep learning approach. Eng. Geol. 288 (106142), 106142. http://dx.doi.org/10.1016/j.enggeo.2021.106142.

Lai, Z., Chen, Q., 2019. Reconstructing granular particles from X-ray computed tomography using the TWS machine learning tool and the level set method. Acta Geotech. 14 (1), 1–18. http://dx.doi.org/10.1007/s11440-018-0759.-x, Springer Vieweg, Berlin, Heidelberg.

Lavrukhin, E.V., Gerke, K.M., Romanenko, K.A., Abrosimov, K.N., Karsanina, M.V., 2021. Assessing the fidelity of neural network-based segmentation of soil XCT images based on pore-scale modelling of saturated flow properties. Soil Tillage Res. http://dx.doi.org/10.1016/j.still.2021.104942.

Li, X., Fan, P., Li, Z., Chen, G., Qiu, H., Hou, G., 2021. Soil classification based on deep learning algorithm and visible near-infrared spectroscopy. J. Spectroscopy. 2021, http://dx.doi.org/10.1155/2021/1508267.

Li, C., Xu, C., Gui, C., Fox, M.D., 2005. Level set evolution without re-initialization: A new variational formulation. In: IEEE Computer Society Conference on Computer Vision and Pattern Recognition (CVPR'05). 43, 0–436. http://dx.doi.org/10.1109/CVPR.2005.213.

Li, C., Xu, C., Gui, C., Fox, M.D., 2010. Distance regularized level set evolution and its application to image segmentation. IEEE Trans. Image Process. 19 (12), 3243–3254. http://dx.doi.org/10.1109/TIP.2010.2069690.

Lianne, J., 2020. Hyperparameter tuning with python: Keras step-by-step guide why and how to use with an example of keras. Just into data. https://www.justintodata.com/hyperparameter-tuning-with-python-keras-guide/ (Accessed 18 April 2021).

Liu, B., Zheng, Q., Zhao, K., Li, H., Ma, C., Wu, S., Tong, X., 2021. HPCSeg-Net: Hippocampus Segmentation Network Integrating Autofocus Attention Mechanism and Feature Recombination and Recalibration Module. In: Lecture Notes in Computer Science, In: Lecture Notes in Computer Science, vol. 12889, 773–782.http://dx.doi.org/10.1007/978-3-030-87358-5_63,

Lu, J., Behbood, V., Hao, P., Zuo, H., Xue, S., Zhang, G., 2015. Transfer learning using computational intelligence: A survey. Knowl.-Based Syst. 80, 14–23. http://dx.doi.org/10.1016/j.knosys.2015.01.010.

Medina, D.A., Jerves, A.X., 2019. A geometry-based algorithm for cloning real grains 2.0. Gran. Matter 21 (1), http://dx.doi.org/10.1007/S10035-018-0851-9.

Meyer, F., 1994. Topographic distance and watershed lines. Signal Process. 38 (1), 113–125. http://dx.doi.org/10.1016/0165-1684(94)90060-4.

Mital, U., Andrade, J.E., 2022. Bridging length scales in granular materials using convolutional neural networks. Comp. Part. Mech. 9, 221–235. http://dx.doi.org/10.1007/s40571-021-00405-1.

Otsu, N., 1979. A threshold selection method from gray-level histograms. IEEE Trans. Syst. Man Cybern. 9 (1), 62–66. http://dx.doi.org/10.1109/tsmc.1979.4310076.

Rawat, W., Wang, Z., 2017. Deep convolutional neural networks for image classification: A comprehensive review. Neural Comput. 29 (9), 2352–2449. http://dx.doi.org/10.1162/NECO_a_00990.

Roverato, M., Larrea, P., Casado, I., Mulas, M., Béjar, G., Bowman, L., 2018. Characterization of the cubilche debris avalanche deposit, a controversial case from the Northern Andes, Ecuador. J. Volcanol. Geotherm. Res. 360, 22–35. http://dx.doi.org/10.1016/j.jvolgeores.2018.07.006.

Shi, J.-J., Zhang, W., Wang, W., Sun, Y.-H., Xu, C.-Y., Zhu, H.-H., Sun, Z.-X., 2021. Randomly generating three-dimensional realistic schistous sand particles using deep learning: Variational autoencoder implementation. Eng. Geol. 291, http://dx.doi.org/10.1016/j.enggeo.2021.106235.

Sivakugan, N., Das, B.M., Sivakugan, S., 2015. Introduction to Geotechnical Engineering. Cengage Learning, United States, http://dx.doi.org/10.1016/B978-0-444-41782-4.50012-9.

Soille, P., 2000. Morphological Image Analysis: Principles and Applications. Springer-Verlag, pp. 170–171. http://dx.doi.org/10.1108/sr.2000.08720cae.001.

Soille, P., 2004. Morphological Image Analysis: Principles and Applications. pp. 173–174. http://dx.doi.org/10.1007/978-3-662-05088-0,

Srivastava, N., Hinton, G., Krizhevsky, A., Sutskever, I., Salakhutdinov, R., 2014. Dropout: A simple way to prevent neural networks from overfitting. J. Mach. Learn. Res.: JMLR 15 (56), 1929–1958, http://jmlr.org/papers/v15/srivastava14a.html.

Stamati, et al., 2020. Spam: Software for practical analysis of materials. J. Open Source Softw. 5 (51), 2286. http://dx.doi.org/10.21105/joss.02286.

Stubbs, T.J., Vondrak, R.R., Farrell, W.M., 2007. Impact of dust on lunar exploration. Dust Planet. Syst. 23, 9–243.

Sun, H.Q., Luo, Y.J., 2009. Adaptive watershed segmentation of binary particle image. J. Microsc. 233 (2), 326–330. http://dx.doi.org/10.1111/j.1365-2818.2009.03125.x.

Tammina, S., 2021. Transfer learning using VGG-16 with deep convolutional neural network for classifying images. Int. J. Sci. Res. Publ. 9 (10), http://dx.doi.org/10.29322/IJSRP.9.10.2019.p9420.

Taner, A., Öztekin, Y.B., Duran, H., 2021. Performance analysis of deep learning CNN models for variety classification in hazelnut. Sustainability 13 (12), http://dx.doi.org/10.3390/su13126527.

Uhl, A., Liedlgruber, M., Butz, K., Höller, Y., Kuchukhidze, G., Taylor, A., Thomschevski, A., Tomasi, O., Trinka, E., 2018. Hippocampus segmentation and SPHARM coefficient selection are decisive for MCI detection. In: Maier, A., Deserno, T., Handels, H., Maier-Hein, K., Palm, C., Tolxdorff, T. (Eds.), Informatik Aktuell. Bildverarbeitung Für Die Medizin, Springer Vieweg, Berlin, Heidelberg, pp. 239–244. http://dx.doi.org/10.1007/978-3-662-56537-7_65.

Viggiani, G., Andò, E., Jaquet, C., Talbot, H., 2013. Identifying and following particle-to-particle contacts in real granular media: an experimental challenge. AIP Conf. Proc. 1542 (1), 60–65. http://dx.doi.org/10.1063/1.4811868.

Vincent, L., Soille, P., 1991. Watersheds in digital spaces: an efficient algorithm based on immersion simulations. IEEE Trans. Pattern Anal. Mach. Intell. 13 (6), 583–598. http://dx.doi.org/10.1109/34.87344.

Vlahinić, I., Andò, E., Viggiani, G., Andrade, J.E., 2014. Towards a more accurate characterization of granular media: extracting quantitative descriptors from tomographic images. Granul. Matter 16 (1), 9–21. http://dx.doi.org/10.1007/s10035-013-0460-6.

Vlahinić, I., Kawamoto, R., Andò, E., Viggiani, G., Andrade, J.E., 2017. From computed tomography to mechanics of granular materials via level set bridge. Acta Geotech. 12, 85–95. http://dx.doi.org/10.1680/geolett.13.00036.

Wiebicke, M., 2020. Experimental analysis of the evolution of fabric in granular soils upon monotonic loading and load reversals. (Ph.D. thesis). Technische Universität Dresden, Germany.

Wiebicke, M., Andò, E., Herle, I., Viggiani, G., 2017. On the metrology of interparticle contacts in sand from x-ray tomography images. Meas. Sci. Technol. 28, http://dx.doi.org/10.1088/1361-6501/aa8dbf.

Xu, Z., Hu, J., Deng, W., 2016. Recurrent convolutional neural network for video classification. In: International Conference on Multimedia and Expo (ICME). Springer-Verlag, pp. 170–171. http://dx.doi.org/10.1109/ICME.2016.7552971.

Zuiderveld, K., 1994. Contrast limited adaptive histogram equalization. Graph. Gems 47, 4–485. http://dx.doi.org/10.1016/B978-0-12-336156-1.50061-6.